Applied Research Laboratory

AD-A280 797

Technical Report

CONDITIONAL PROBABILITY DENSITY FUNCTIONS ARISING IN BEARING ESTIMATION

by

M. J. Roan
J. E. Dzielski

DTIC
ELECTE
JUN 2 9 1994
S F D

This document has been approved for public release and sale; its distribution is unlimited.

PENNSTATE

94-19806

The Pennsylvania State Uni . sity
APPLIED RESEARCH LABORATORY
P.O. Box 30
State College, PA 16804

CONDITIONAL PROBABILITY DENSITY FUNCTIONS ARISING IN BEARING ESTIMATION

by

M. J. Roan
J. E. Dzielski

DTIC QUALITY INSPECTED 2

Technical Report No. TR 94-09
May 1994

DTIC
ELECTE
JUN 2 9 1994
S F D

Supported by:
Space and Naval Warfare Systems Command

L.R. Hettche, Director
Applied Research Laboratory

Approved for public release; distribution unlimited

94 6 28 159

REPORT DOCUMENTATION PAGE

Form Approved
OMB No. 0704-0188

Public reporting burden for this collection of information is estimated to average 1 hour per response, including the time for reviewing instructions, searching existing data sources, gathering and maintaining the data needed, and completing and reviewing the collection of information. Send comments regarding this burden estimate or any other aspect of this collection of information, including suggestions for reducing this burden, to Washington Headquarters Services, Directorate for Information Operations and Reports, 1215 Jefferson Davis Highway, Suite 1204, Arlington, VA 22202-4302, and to the Office of Management and Budget, Paperwork Reduction Project (0704-0188), Washington, DC 20503.

1. AGENCY USE ONLY (Leave blank)	2. REPORT DATE	3. REPORT TYPE AND DATES COVERED
	May 1994	

4. TITLE AND SUBTITLE
Conditional Probability Density Functions Arising in Bearing Estimation

5. FUNDING NUMBERS

6. AUTHOR(S)
M. J. Roan, J. E. Dzielski

7. PERFORMING ORGANIZATION NAME(S) AND ADDRESS(ES)
Applied Research Laboratory
The Pennsylvania State University
P.O. Box 30
State College, PA 16804

8. PERFORMING ORGANIZATION REPORT NUMBER
TR-94-09

9. SPONSORING/MONITORING AGENCY NAME(S) AND ADDRESS(ES)
Space and Naval Warfare Systems Command
2451 Crystal Drive
Arlington, VA 22245-5200

10. SPONSORING/MONITORING AGENCY REPORT NUMBER
N00039-92-C-0100

11. SUPPLEMENTARY NOTES

12a. DISTRIBUTION/AVAILABILITY STATEMENT
Unlimited

12b. DISTRIBUTION CODE

13. ABSTRACT *(Maximum 200 words)*

The aim of this thesis is to calculate and discuss some of the properties of probability density functions of bearing angle conditioned on the data received by an array of sensors.

The development of the thesis goes through three major stages. The first stage of the development is the theoretical derivation of the probability density function. The second stage of the development concerns the calculation of the density function with examples. This development includes a detailed discussion of the simulation used to produce the data on which the density functions are conditioned and the code written to do the actual computations. The third stage of the development is the analysis of estimates which are made using the calculated density functions. This stage includes comparison of the results obtained using the calculated density functions and a better known performance measure: the Cramer-Rao bound.

14. SUBJECT TERMS
Probability Density Function, bearing angle estimation

15. NUMBER OF PAGES
87

16. PRICE CODE

17. SECURITY CLASSIFICATION OF REPORT	18. SECURITY CLASSIFICATION OF THIS PAGE	19. SECURITY CLASSIFICATION OF ABSTRACT	20. LIMITATION OF ABSTRACT
UNCLASSIFIED	UNCLASSIFIED	UNCLASSIFIED	UNLIMITED

Abstract

The aim of this thesis is to calculate and discuss some of the properties of probability density functions of bearing angle conditioned on the data received by an array of sensors.

The development of the thesis goes through three major stages. The first stage of the development is the theoretical derivation of the probability density function. The second stage of the development concerns the calculation of the density function with examples. This development includes a detailed discussion of the simulation used to produce the data on which the density functions are conditioned and the code written to do the actual computations. The third stage of the development is the analysis of estimates which are made using the calculated density functions. This stage includes comparison of the results obtained using the calculated density functions and a better known performance measure: the Cramer-Rao bound.

The major results obtained are as follows. The first major result is that the density functions of bearing conditioned on the actual data received at an array of sensors are skewed as bearing angle increases from the 0° array centerline. Better estimates are obtained for more samples, better sampling resolution, or higher SNR. The final result is that the error variances of estimates made using the density functions calculated decrease with increasing sample number, SNR, and sampling resolution.

Table of Contents

Page

List of Figures.....vii

List of Symbols.....ix

Chapter

1 Outline and Goals.....1

1.1 Introduction.....1

1.2 Historical Perspective.....2

1.3 Goals of the Thesis.....4

2 Calculation of the Density Function.....6

2.1 Introduction.....6

2.2 Signal Model.....7

2.3 Development of the Covariance Matrix.....10

2.4 Inclusion of Additive Noise and the Density Function.....14

2.5 Computation of the Covariance Matrix.....17

2.6 Description of the Code.....21

2.7 Summary and Results.....23

Accesion For
NTIS CRA&I ☒
DTIC TAB ☐
Unannounced ☐
Justification .....
By .....
Distribution /
Availability Codes
Dist | Avail and / or Special
A-1

Table of Contents (continued)

3 Discussion of the Simulation and Examples of Density Functions.....25

3.1 Introduction.....25

3.2 Simulation of Signal and Noise.....27

3.3 Signal - to - Noise Ratio.....31

3.4 Analysis of Simulation Outputs.....32

3.5 Example 1: Effect of Change in Bearing on the Density Function.....37

3.6 Example 2: Effect of Sensor Separation on the Density Function.....40

3.7 Example 3: Effect of the Number Samples per Sensor on the Density Function.....42

3.8 Example 4: Effect of the Signal-to-Noise Ratio on the Density Function.....43

3.9 Summary and Results.....45

Table of Contents (continued)

4 The Conditional Density Function and Bearing Estimation.....47

4.1 Introduction.....47

4.2 Discussion of the Simulation.....48

4.3 Discussion of the Covariance Matrix.....50

4.4 Estimation of Bearing Angle.....54

4.5 Statistics of the Estimates.....58

4.6 Summary and Results.....70

5 Conclusions and Recommendations.....72

5. Introduction.....72

5.2 Conclusions and Results.....72

5.3 Recommendations for Further Investigation.....77

References.....79

Appendix A.....80

Appendix B.....86

List of Figures

Figure Page

1. Receiver and Signal Geometry..... 9

2. Model for Sensor Array.....25

3. Schematic for Simulation of Data.....28

4. Sample Output of MATRIXx Simulation.....30

5. Frequency Response of the Filter.....30

6. Output of Noise Generator.....33

7. Autocorrelation of the Noise Sequence.....34

8. Probability Density Functions for Varying Bearing Angles.....38

9. Varying Density Functions For Different Data Sets.....39

10. Probability Density vs. Bearing Angle for Varying Sensor Separation Distances.....41

11. Probability Density vs. Bearing Angle for Varying Sensor Separation Distances.....41

12. Density Functions for Varying Numbers of Samples/Sensor.....42

13. Density Functions for a Change in Signal-to-Noise Ratio.....44

14. Schematic for Data Simulation.....48

15. Sampling Interval, Propagation Delay, and Covariance Singularities.....52

List of Figures (continued)

Figure Page

16. Condition Number of Covariance vs. Bearing Angle.....53

17. Estimate vs. Bearing Angle (10 Samples/Sensor at 2 Sec Intervals).....56

18. Estimate vs. Bearing Angle (20 Samples/Sensor at 1 Sec Intervals).....56

19. Estimate vs. Bearing Angle (20 Samples/Sensor at 0.5 Sec Intervals).....57

20. Estimate Variance vs. Bearing Angle (10 Samples/Sensor 2 sec Interval).....64

21. Estimate Variance vs. Bearing Angle (20 Samples/Sensor 1 sec Interval).....65

22. Estimate Variance vs. Bearing Angle (20 Samples/Sensor 0.5 sec Interval).....66

23. Averaged Density Functions (10 Samples/Sensor 2 sec Interval).....68

List of Symbols

A	An experimental event.
$Prob(A)$	Probability Associated with event A.
X	General Random Variable.
p_X	Probability Density Function of Random Variable X.
Y	Observation of Random Variable X.
$p_{X\|Y}$	Probability Density Function of X Conditioned on Y.
ψ	Bearing Angle To a Source.
n	Number of Sensors.
P_n	Number of Samples Taken at Sensor n.
$S_n(t)$	Signal Received at Sensor n.
$S_o(t)$	Signal Received at the Reference Sensor.
d	Distance Between Sensors.
τ_n	Propagation Delay Between Sensor n and Reference Sensor.
c	Speed of Sound in the Medium.
R_{So}	Autocorrelation of Signal at the Reference Sensor
$R_{SS}(\psi)$	Covcariance Matrix of S.
$p_{S\|\psi}$	Probability Density Function of S Conditioned on ψ.
$m/2$	Total Number of Samples Taken at All of the Sensors.
Y_i	Total Signal at the i'th Sensor.
S_i	Signal Component at the i'th Sensor.

List of Symbols (continued)

N_i	Noise Component at the i'th Sensor.
$R_{YY}(\psi)$	Covariance of the Data.
P_n	Number of Samples Taken at n'th Sensor.
E[X]	Expected Value of X.
D	Delay Matrix.
SNR	Signal-to-Noise Ratio.
σ_S^2	Variance of Signal S.
μ_s	Mean Value of Signal S.
R_{NN}	Covariance of the Noise.
Δt	Output interval of the Simulation.
σ_Y^2	Variance of the Total Signal.
ω	Radian Frequency.
$H(\omega)$	Frequency Response of the Filter.
$S_{XX}(\omega)$	Autospectrum of X.
σ_N^2	Variance of the Noise.
t_s	Sensor Sampling Interval.
λ	Filter Center Frequency Wavelength.
μ_ψ	Mean Value of the Bearing.
MAP	Maximum A Posteriori Estimation.
MMSE	Minimum Mean Square Estimation.

σ_{CR}^2	Cramer-Rao Lower Bound.

Chapter 1 Outline and Goals

1.1 Introduction

The work in this thesis is developed in order to calculate and explore the properties of probability density functions of the bearing angle to a source conditioned on data sampled at the outputs of an array of sensors. The thesis begins with the theoretical background for the computation of the density functions. This includes a close examination of the covariance matrix of the data. The development then turns to the actual computation of the density functions, the code used to construct the covariance matrix and the generation of simulated data for use in the calculations. The next step in the development is the computation of some examples for various sampling schemes and sensor geometries. The next part of the thesis includes a more complicated noise model in the simulation of the data and in the covariance calculation. Following this is a discussion of the estimation of the bearing angle using various techniques and also using the density functions calculated previously. A bound on the estimate of the variance, the Cramer-Rao bound, is calculated and compared to statistics calculated from the density functions. The last part of the thesis is a review of the results obtained and recommendations for further research in the area.

1.2 Historical Perspective

The problem of determining the direction of arrival of wavefronts generated by a source in the presence of noise has been discussed extensively in the literature. The earliest beginnings lie as far back as Leonardo de Vinci who noted that one can hear distant ships by placing one end of an air filled tube into the water and placing the other to the ear.

The onset of WWI really began the explosion of development of acoustical devices for detecting and localizing a source. The British and French are credited with the fist application of acoustical tracking devices to detect enemy aircraft and zeppelins. The developments made in these areas were later applied to the detection of underwater sound sources. Early devices were connected directly to a human operators ear via a stethoscope. Devices such as the American SC tube and the MB tube are examples of early successful detection and localization equipment (Burdic, 1989, pp.22-23).

The development of vacuum tube technology during WWII helped to improve the performance of systems designed for detection purposes. Also during the war, the work of Norbert Wiener and S.O. Rice in brought communications theory into a new era. Methods of separating a signal from the noise in which it is embedded began to mature with the work of Shannon, Gabor, and Woodwind (Burdic, 1989, pp.22-23).

With the end of WWII, the onset of the cold war spawned developments such as the atom bomb, ballistic missiles, and the submarine-launched missile. These new systems made the detection and tracking of sources a major priority throughout the world.

With the development of the digital computer through the late 60's and the 70's, the use of the computer has fully taken over the job of tracking. Hence, many algorithms have been developed to solve the direction-of-arrival problem. Three main types of algorithms have been developed. The first are known as "signal subspace" methods. The relationship between the array geometry and the direction of arrival can be characterized by a clearly defined structure of the covariance matrix. The signal subspace methods exploit the structure of the covariance to determine the direction of arrival. The second class of direction of arrival algorithms are known as beamforming techniques. In these methods, sensor weights and tapped delays are used in order to alter the sensitivity of the array in specific directions. The way in which the weights are selected determines the nature of the algorithm. A third class of algorithms are called spectral estimation techniques. Spectral estimation techniques utilize the relationship between estimates of discrete frequencies in a time series and spatial wavenumbers associated with an interference pattern. These techniques often base the model of the received signal on a state space model and adopt the model to match the signal.

In the Bayes' approach to estimation, a cost function which is a function of the error is optimized using statistics computed from the conditional a posterior probability function. When the signal and noise processes are Gaussian, and the signal parameters can be accurately estimated, the minimum variance and maximum likelihood estimators closely approximate each other. When the SNR is low or when the array geometry or medium contain uncertainties, it is necessary to obtain the direction of arrival density function conditioned on the actual data at the sensor outputs. With the directly calculated density function, algorithms can be used to optimize statistics of the direction of arrival estimate.

1.3 Goals of the Thesis

There are three main goals of the thesis. The first goal is to present the rigorous development of the theory involved in the calculation of the probability density function of direction of arrival conditioned on the data sampled at an array of sensors. The second goal of the thesis is to show how the density functions behave when various parameters of array geometry and sampling scheme are varied. By observing how the density functions change as a function of bearing it is shown that the density functions of bearings near 0° appear Gaussian while densities near $\pm 90^\circ$ are far from Gaussian. The third and final goal of the thesis is to give a detailed discussion of the estimation of direction of arrival using the densities calculated above.

The variances of the estimates of bearing are then compared to the Cramer-Rao bound. This is done in order to give a comparison of performance of a Bayes' optimal estimator with the C-R bound.

Chapter 2 Calculation of the Density Function

2.1 Introduction

In this chapter an analytical formula is developed for the probability density of the direction to a source in the far field of a array of sensors. The density function is conditioned on a finite set of sensor outputs. Both the signal and corrupting noise are assumed to be zero-mean Gaussian random processes. First, a model of the signal is developed. This development includes the sensor geometry and sampling scheme. The development of the signal model begins with the signal alone then is expanded to include the noise process. It is shown, through a discussion of the correlation function, how the signal and noise processes are characterized. The development of the observation model is discussed next and goes through four stages. First, the continuous time signal received at each sensor is discussed. This leads to a discussion of the signal received at each sensor in terms of the signal received at a reference location. The signal received at the reference location is related to the signal at each of the sensors by the propagation delay between sensors. Third, the time sampling of the signal is included in the observation model. Fourth, the inclusion of additive noise is discussed. After the noise characterization model, the density function of the signal conditioned on the direction of arrival is presented. Through the application of Bayes' Rule to this density, the density function of direction of arrival conditioned on

the set of observations is produced. The most involved portion of the development of the above density function is the development of the covariance matrix. A detailed discussion of the covariance matrix is presented. This includes the relationship between the covariance matrix and the autocorrelation of the signal received at the reference location. Finally, a description of an algorithm for the construction of the covariance and conditional density function is presented.

In the following discussion the notation to be used is as follows. The probability associated with an event, A, will be denoted Prob(A). Random variables will be denoted by upper case letters and the result of an experiment will be denoted by a lower case letter. A probability density is denoted by a lower case p, with an upper case subscript to denote the random variable. For example, p_X is the probability density associated with the random variable X, and $p_X(a)$ is the probability density function of the random variable X evaluated at a. A conditional random variable is denoted by a vertical bar. For example, $p_{X|Y}$ is the probability density of the random variable X conditioned on the observation Y.

2.2 Signal Model

The purpose of this section is to present the development of the covariance matrix. In order to fully develop the covariance, a model of the signal and explanation of the sensor geometry is necessary. It is assumed that there is a source producing an

acoustic signal located in a medium. This signal can be a complicated combination of signals from a complex source. Examples would include machinery noise, bearing or rotation noise, flow noise, or a complicated combination of all of these. The source could produce a random signal in Gaussian background noise or a sinusoid with high signal to noise ratio. The only assumption made on the signal and noise is that both are zero mean, Gaussian processes.

The signal and noise are received by an array of sensors. The array can be a two-dimensional array of n sensors or a linear array. For the purpose of simplicity, the rest of the discussion assumes a linear array of n elements. The source discussed above is assumed to be in the far field of the array so that the signal arrives in the form of plane waves across the array as seen in Figure 1.

The geometry of the array is shown in Figure 1 as an n element array, with separation distance d between sensors. The signal arrives in the form of plane waves and arrives at bearing angle ψ.

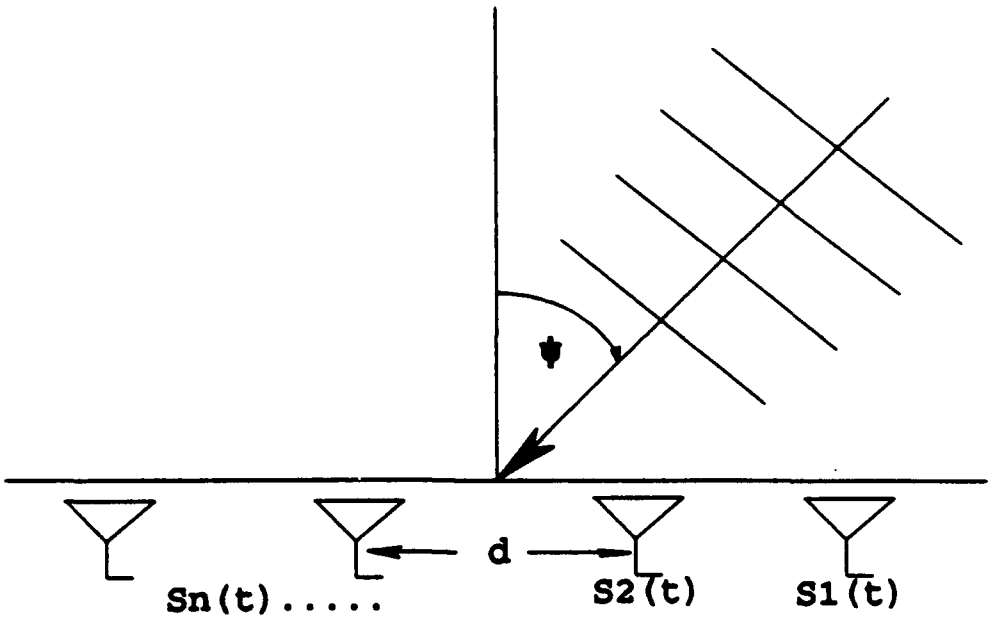

Figure 1: Receiver and Signal Geometry

The signal is a continuous time process which is discretized both spatially and temporally. The signal is spatially 'sampled' due to the fact that there is a finite distance between sensors. The signal is discretized temporally by digitally sampling the signal. The sampling interval can either fixed or variable length. The development of the covariance which follows begins with the signal at an individual sensor and is expanded to include multiple samples taken at all of the sensors. The discussion is further expanded to include the noise process in the following section.

2.3 Development of the Covariance Matrix

The signal received at each of the sensors is denoted by the symbol $S_n(t)$ [n=1,2,3,...]. $S_1(t)$ denotes the signal received at an arbitrary reference sensor. The signal at this arbitrary reference sensor is related to the signals received at the other sensors by the propagation delay between sensors. The relation between the signal received at the reference sensor (sensor 1) and at the other sensor locations assuming the geometry in Figure 1 is given by $S_n(t)=S_1(t-\tau_n)$ where

$$\tau_n = \frac{n\,d\sin(\psi)}{c} \tag{1}$$

d is the distance between neighboring sensors, ψ is the bearing angle, and c is the sound speed in the medium. While only a linear array of n elements is shown and planar wavefronts are assumed, the results presented can be readily generalized to a two dimensional array with the sensors having arbitrary separation distance and the signal arriving with curved wavefronts by modification of (1).

Assuming that the signal is zero mean and Gaussian, the process is characterized by its autocorrelation function $R_{s1}(t_1)$. Given the autocorrelation $R_{s1}(t_1)$, pair-wise joint processes of the form $[S_i(t_1)\ ,\ S_j(t_1)]$ can be characterized by the matrix valued autocorrelations:

$$R_{S_i S_j}(t_1,t_2) = \begin{bmatrix} R_{S_i}(t_1-\tau_i, t_1-\tau_i) & R_{S_i}(t_1-\tau_i, t_1-\tau_j) \\ R_{S_i}(t_1-\tau_i, t_1-\tau_j) & R_{S_i}(t_1-\tau_j, t_1-\tau_j) \end{bmatrix} \quad (2)$$

The process $[S_i(t_1)\ ,\ S_j(t_1)]$ is a model for sampling of the signal once at each on the sensors i and j at times t_1. Equation (2) is arrived at by noting that the signal received at a given element is related to the signal at the reference sensor by a time shift. The dependance on ψ can be incorporated into (2) by the relation (1). The autocorrelations (2) can be extended to joint processes of a signal received at a number of sensors n. Here t_1 denotes the time at which the sensors are sampled. The vector valued process can be characterized by: $\bar{S}(t_1) \triangleq [S_1(t_1), S_2(t_1), \ldots, S_n(t_1)]^T$ which has the autocorrelation function:

$$R_{\bar{S}}(t_1;\psi) = \begin{bmatrix} R_{S_1}(t_1-\tau_1, t_1-\tau_1) & \ldots\ldots & R_{S_1}(t_1-\tau_n, t_1-\tau_1) \\ \cdot & & \cdot \\ \cdot & & \cdot \\ \cdot & & \cdot \\ R_{S_1}(t_1-\tau_1, t_1-\tau_n) & \ldots\ldots & R_{S_1}(t_1-\tau_n, t_1-\tau_n) \end{bmatrix} \quad (3)$$

On examination of (3) it is seen that the autocorrelation is parameterized by $\{t_1\}$ and τ_n. Explicit dependence in (3) on the bearing angle ψ is accomplished via (1).

The probability density function of the random variable $\bar{S}(t_1)$ conditioned on the bearing angle ψ is given by:

$$p_{\bar{S}|\psi}(S_1(t_1),.....S_n(t_1)|\psi)=\frac{1}{(2\pi)^{n/2}|R_{\bar{S}(t_1)}|^{1/2}}Exp[-\frac{1}{2}\bar{S}(t_1)^T R_{\bar{S}(t_1)}{}^{-1}(t_1;\psi)\bar{S}] \qquad (4)$$

It is seen that the inverse of the covariance (3) is needed in (4). There are a number of possible bearings ψ_0 for which the inverse of the covariance does not exist. In the following discussion, when a density function of the form (4) appears, its existence depends on the value of bearing ψ and the value of the density at ψ_o is understood to be defined by a limit taken as ψ approaches ψ_o since $p_{\bar{S}|\psi}$ fails to exist only for isolated values of ψ. It is also recognized that when a density function of the form (4) appears, it will appear in an expression involving an integral over a quadrant of its domain. This characterizes a distribution of the form

$$Prob(X<a) = \int_{-\infty}^{a} p_X(x)\,dx \qquad (5)$$

and is always well defined.

The covariance (3) must now be generalized further to include multiple samples taken at each sensor. The covariance (3) characterizes the case of one sample taken at

each sensor. For the purposes of the work done here, the same number of samples are taken at each sensor and the samples are taken at uniform sampling intervals. In general, however, the samples need not be taken at the same time nor must the same number of samples be taken at each sensor. The set of sampled values described by the vector $\bar{S}$ can now be written:

$$\bar{S}(\bar{t}) = [S_1(t_1),\ldots,S_1(t_{p_1}),S_2(t_1),\ldots,S_2(t_p),\ldots,S_n(t_1),\ldots,S_n(t_p)]^T \tag{6}$$

Here $t=[t_1, \ldots t_p]$ is the set of p times that each sensor is sampled, and $\bar{S}$ is a finite, jointly distributed, Gaussian random variable. The covariance of $\bar{S}=\bar{S}(\bar{t})$ is given by

$$R_{\bar{S}\bar{S}}(\psi) = E[\bar{S}\bar{S}^T] \tag{7}$$

which can be determined by using the autocorrelation of the reference sensor $R_{s1}(t_1)$ at the appropriate times. The density function of $\bar{S}$ conditioned on ψ is:

$$p_{\bar{S}|\psi} = \frac{1}{(2\pi)^{\frac{m}{2}} |R_{\bar{S}\bar{S}}|^{\frac{1}{2}}} Exp(-\frac{1}{2}\bar{S}^T R_{\bar{S}\bar{S}}^{-1}(\psi)\,\bar{S}) \tag{8}$$

where m is the total number of samples taken at all of the sensors.

2.4 Inclusion of Additive Noise and the Density Function

To further generalize the discussion, the inclusion of an additive noise process will now be discussed. The model for the signal at the i'th sensor is

$$\bar{Y}_i(\bar{t}) = \bar{S}_i(\bar{t}) + \bar{N}_i(\bar{t}) \tag{9}$$

The noise process $\bar{N}(t)=[N_1(t_1)\ldots N_1(t_p),N_2(t_1)\ldots N_2(t_p),N_n(t_1)\ldots N_n(t_p)]^T$ is assumed to be a jointly Gaussian process. Since the signal and noise are assumed to be jointly Gaussian, the joint process $[\bar{S}^T(\bar{t}),\bar{N}^T(\bar{t})]^T$ is characterized by the autocorrelation function

$$R(\bar{t};\psi) = \begin{bmatrix} R_{\bar{S}\bar{S}}(\bar{t};\psi) & R_{\bar{S}\bar{N}}(\bar{t};\psi) \\ R_{\bar{N}\bar{S}}(\bar{t};\psi) & R_{\bar{N}\bar{N}}(\bar{t}) \end{bmatrix} \tag{10}$$

Sampling the sensor outputs as described by (9) is an observation of the joint process described by (10). Using (6) to describe the sampled signal and a similar expression to define the sampled noise process, the density of the finite random variable $[\bar{S}^T,\bar{N}^T]^T$ is characterized by the large covariance matrix which includes time samples

$$R(\psi) = \begin{bmatrix} [R_{\bar{S}\bar{S}}(\psi)] & [R_{\bar{S}\bar{N}}(\psi)] \\ [R_{\bar{N}\bar{S}}(\psi)] & [R_{\bar{N}\bar{N}}] \end{bmatrix} \tag{11}$$

In general, $R_{\bar{s}\bar{s}}^{-1}(\psi)$ is singular for certain values of ψ. Reasons for this are presented in Chapter 4. The submatrix $R_{\bar{N}\bar{N}}(\psi)$ may contain correlated elements, but usually contains an uncorrelated component. $R_{\bar{s}\bar{N}}$ and $R_{\bar{N}\bar{s}}$ will be zero if the signal and noise are uncorrelated. The density function of $\bar{S}$ and $\bar{N}$ conditioned on ψ is given by

$$p_{\bar{S},\bar{N}|\psi}(\bar{S},\bar{N}|\psi) = \frac{1}{(2\pi)^m |R(\psi)|^{\frac{1}{2}}} \exp\left[-\frac{1}{2}[\bar{S}^T \bar{N}^T]^T R^{-1}(\psi)\begin{bmatrix}\bar{S}\\ \bar{N}\end{bmatrix}\right] \tag{12}$$

The total input received is defined as the random variable

$$\bar{Y} = \bar{S} + \bar{N} \tag{13}$$

The covariance of $\bar{Y}$ is obtained from (11) using (13) in the following manner. The vector $\bar{X}$ is defined as

$$\bar{X} = \begin{bmatrix}\bar{S}\\ \bar{N}\end{bmatrix} \tag{14}$$

Using the definition of $\bar{X}$ (13) can be written as

$$\bar{Y} = [\bar{I}\,\bar{I}]\bar{X} \tag{15}$$

The covariance of the data is given by

$$R_{\bar{Y}\bar{Y}} = E[\bar{Y}\,\bar{Y}^T] \tag{16}$$

or combining (14) and (15)

$$R_{\bar{Y}\bar{Y}} = [\bar{I}\,\bar{I}]\,E[\bar{X}\,\bar{X}]\begin{bmatrix}\bar{I}\\ \bar{I}\end{bmatrix} \tag{17}$$

Where $E[\bar{X}\bar{X}]$ is the covariance of the vector defined by (14). Therefore, (17) can be written as

$$R_{\bar{Y}\bar{Y}} = [\bar{I}\bar{I}]\,R_{\bar{X}\bar{X}}\begin{bmatrix}\bar{I}\\ \bar{I}\end{bmatrix} \tag{18}$$

or

$$R_{\bar{Y}\bar{Y}} = R_{\bar{S}\bar{S}} + R_{\bar{N}\bar{S}} + R_{\bar{S}\bar{N}} + R_{\bar{N}\bar{N}} \tag{19}$$

Using Bayes' Rule with (19) the probability density function for direction of arrival conditioned on the actual samples of the sensor outputs is obtained. The result is

$$p_{\psi|\bar{Y}}(\psi\,|\,\bar{y}) = \frac{p_{\bar{Y}|\psi}(\bar{y}\,|\,\psi)\,p_{\psi}(\psi)}{p_{\bar{Y}}(\bar{y})} \tag{20}$$

Here $p_{\psi}(\psi)$ is a prior density function on bearing which is in general not Gaussian.

2.5 Computation of the Covariance Matrix

In this section the structure of the covariance $R(\psi)$ appearing in (12) is discussed. It was stated that the covariance (11) is constructed by evaluation of the autocorrelation of the signal received at the reference sensor at the appropriate times t_1 , t_2. In this section a matrix of the appropriate delays will be constructed by closely examining (7). By selecting values of the autocorrelation of the signal received at the reference sensor which correspond to the delays in the delay matrix, the covariance is constructed.

It was shown that $R(\psi) = E[\bar{S}\bar{S}^T]$ where the signal $\bar{S}$ is given by (6). Expanding the matrix notation we see

$$SS^T = \begin{bmatrix} S_1(t_1)S_1(t_1) & S_1(t_1)S_1(t_2) & \cdots\cdots & S_2(t_1)S_1(t_1) & \cdots\cdots & S_n(t_p)S_1(t_1) \\ S_1(t_2)S_1(t_1) & \cdots & \cdots & \cdots & \cdots & \cdot \\ \cdot & \cdot & \cdot & \cdot & \cdot & \cdot \\ \cdot & \cdot & \cdot & \cdot & \cdot & \cdot \\ \cdot & \cdot & \cdot & \cdot & \cdot & \cdot \\ S_1(t_p)S_1(t_1) & \cdots & \cdots & \cdots & \cdots & S_2(t_1)S_2(t_1) \\ S_2(t_1)S_1(t_1) & \cdots & \cdots & \cdots & \cdots & S_1(t_p)S_1(t_1) \\ \cdot & \cdot & \cdot & \cdot & \cdot & \cdot \\ \cdot & \cdot & \cdot & \cdot & \cdot & \cdot \\ \cdot & \cdots & \cdots & \cdots & \cdots & S_1(t_2)S_1(t_1) \\ S_n(t_p)S_1(t_1) & \cdots & \cdots & \cdots & \cdots & S_n(t_p)S_n(t_p) \end{bmatrix} \quad (21)$$

Taking the expected value of (21) will produce the covariance. In order to evaluate the covariance it is first necessary to put each individual element in (21) in terms of the reference sensor autocorrelation $R_{s1}(t_1 , t_2)$. In order to better illustrate the point of creating the matrix of delays a few examples will be given. In order to simplify the notation, it is assumed that the signal $S_1(t)$ is stationary and $R_{s1}(t_1 , t_2) = R_{s1}(0,t_1-t_2)$ or the autocorrelation is if the form $R_{s1}(\tau)$.

$$E[S_1(t_1)S_1(t_1)] = E[S_1(t_1)S_1(t_1+0)] = R_{S_1}(0) \quad (22)$$

$$E[S_2(t_1)S_1(t_1)] = E[S_1(t_1+\tau_{12})S_1(t_1)] = R_{S_1}(\tau_{12}) \quad (23)$$

$$E[S_1(t_2)S_1(t_1)] = E[S_1(t_1+\Delta t)S_1(t_1)] = R_{S_1}(\Delta t) \tag{24}$$

In the Equations (22), (23), and (24) the symbol R_{s1} denotes the autocorrelation of the signal at the reference sensor. The symbol Δt is the sampling interval in seconds. The symbol τ_{ij} is the propagation delay between the sensors i and j for a given direction of arrival is given by

$$\tau_{ij} = \frac{d_{ij}\sin(\psi)}{c} \tag{25}$$

Completing the above for all of the elements in the delay matrix and denoting the delay matrix D results in the matrix

$$D=\begin{bmatrix} 0 & \Delta t_1 & 2\Delta t_1 & \cdots\cdots & p_1\Delta t_1 & \tau_{12} & \tau_{12}+2\Delta t_2 & \cdots\cdots & \tau_{1n}+p_n\Delta t_n \\ -\Delta t_1 & 0 & \Delta t_1 & \cdot & \cdot & \cdot & \cdot & \cdot & \cdot \\ -2\Delta t_1 & -\Delta t_1 & 0 & \cdot & \cdot & \cdot & \cdot & \cdot & \cdot \\ \cdot & \cdot & \cdot & \cdot & \cdot & \cdot & \cdot & \cdot & \cdot \\ \cdot & & & & & & & & \\ \cdot & & & & & & & & \\ -p_n\Delta t_1 & & & & & & & & \\ -\tau_{12} & & & & & & & & \\ -\tau_{12}-\Delta t_2 & & & & & & & & \\ -\tau_{12}-2\Delta t_2 & & & & & & & & \\ \cdot & & & & & & & & \\ \cdot & & & & & & & & \\ \cdot & \cdot & \cdot & \cdot & \cdot & \cdot & \cdot & \cdot & \Delta t_1 \\ -\tau_{1n}-p_n\Delta t_n & \cdot & \cdot & \cdot & \cdot & \cdot & \cdot & \cdot & 0 \end{bmatrix} \quad (26)$$

By matching the delays in the above matrix (26) with the delays in the autocorrelation of the reference sensor $R_{s1}(\tau)$ the covariance matrix is constructed.

It is seen that the delay matrix is skew symmetric about a main diagonal of zeroes. The covariance, however, will be symmetric due to the symmetry of the autocorrelation. The covariance $R(\psi)$ is obtained by addition of $R_{\hat{n}\hat{n}}$ to $R_{\hat{s}\hat{s}}$ assuming that the signal and noise are uncorrelated so that $R_{\hat{s}\hat{n}}$ and $R_{\hat{n}\hat{s}}$ are zero. More discussion of the covariance is given later in relation to specific noise models.

2.6 Description of the Code

In order to calculate the density (20), a computer program was written to compute, for each ψ, the covariance $R_Y^{-T}(\psi)$, the inverse $R_Y^{-T-1}(\psi)$, and the determinant $\mathrm{Det}(R_Y^{-T}(\psi))$ and pre- and post-multiply the inverse by the vector of sampled values. The possible bearings are considered for a linear array of sensors with equal spacing which are sampled at the same time with the same sampling intervals at each sensor. The range of possible bearings is $-\pi/2$ to $\pi/2$ radians since for a linear array, reciprocal bearings are expected and a "forward looking" array will be considered.

The covariance and its inverse must be constructed in order to calculate the density (20). In order to accomplish this, two main steps are taken. The first is to construct a matrix of delays which are based on the propagation delays between sensors and the sampling interval at the sensor outputs. The second is to match the delays in the delay matrix to the delays in the autocorrelation of the reference sensor and place the corresponding autocorrelation in the position of the matching delay.

The matrix of delays is constructed from groups of submatrices. Symmetry within the covariance greatly reduces the number of actual elements in the delay matrix to be filled. For the case of equal numbers of samples taken at all of the sensors, the covariance matrix is a square matrix with dimensions [n*P x n*P] where n is the number of sensors and P is the number of samples taken at each sensor. Upon close

examination of (26) it is seen that the subblocks which make up the main diagonal are identical. The subblocks containing the main diagonal are calculated from the sampling interval and number of samples taken at the reference sensor. This means that there are no cross-terms in the main diagonal subblocks and that the delay between the sensors given by (25) does not appear in the main-diagonal subblocks. It is necessary only to calculate one such subblock and to place it into positions along the main diagonal of the delay matrix. In calculating the main-diagonal subblocks, it is necessary due to symmetry only to fill the elements which lie below the main diagonal of zeroes. By filling the elements below the main diagonal with the proper delay values and all other elements with zeroes, the subblock is calculated by adding the negative of the transpose of the half-filled subblock to the half-filled subblock. It should be noted the number of subblocks is n^2 where n is again the number of sensors. It is also seen that the subblocks which lie above the main diagonal of subblocks are the transposes of those lying below the main diagonal subblocks. Equation (27) gives an example of the delay matrix for two sensors in a linear array taking four samples at a rate of t_s.

$$D = \begin{bmatrix} \begin{bmatrix} 0 & t_s & 2t_s & 3t_s \\ -t_s & 0 & t_s & 2t_s \\ -2t_s & -t_s & 0 & t_s \\ -3t_s & -2t_s & -t_s & 0 \end{bmatrix} & \begin{bmatrix} \tau_{12} & \tau_{12}+t_s & \tau_{12}+2t_s & \tau_{12}+3t_s \\ \tau_{12}-t_s & \tau_{12} & \tau_{12}+t_s & \tau_{12}+2t_s \\ \tau_{12}-2t_s & \tau_{12}-t_s & \tau_{12} & \tau_{12}+t_s \\ \tau_{12}-3t_s & \tau_{12}-2t_s & \tau_{12}-t_s & \tau_{12} \end{bmatrix} \\ \begin{bmatrix} -\tau_{12} & -\tau_{12}+t_s & -\tau_{12}+2t_s & -\tau_{12}+3t_s \\ -\tau_{12}-t_s & -\tau_{12} & -\tau_{12}+t_s & -\tau_{12}+2t_s \\ -\tau_{12}-2t_s & -\tau_{12}-t_s & -\tau_{12} & -\tau_{12}+t_s \\ -\tau_{12}-3t_s & -\tau_{12}-2t_s & -\tau_{12}-t_s & -\tau_{12} \end{bmatrix} & \begin{bmatrix} 0 & t_s & 2t_s & 3t_s \\ -t_s & 0 & t_s & 2t_s \\ -2t_s & -t_s & 0 & t_s \\ -3t_s & -2t_s & -t_s & 0 \end{bmatrix} \end{bmatrix} \quad (27)$$

Once the delay matrix is filled, the covariance is constructed by matching the delays in the delay matrix to the delays in the autocorrelation of the signal received at the reference sensor. The autocorrelation of the signal at the reference sensor is sampled and stored in a data vector. In practice, the matching is accomplished by executing a binary search on the data vector for each delay put into the delay matrix (27). This is done so that the symmetry of the autocorrelation can be exploited to reduce the computation time, since only half of the elements must be searched.

The above must be completed for each bearing angle of interest since the propagation delay between sensors used in constructing the covariance is a function of bearing angle.

2.7 Summary of Chapter 2

In this chapter the formulation of the probability density function of direction-of-arrival conditioned on the actual sample values taken at each of the sensors has been developed. The result was arrived at by development of the density function of the signal conditioned on the bearing angle and the use of Bayes' rule to arrive at the density function of bearing angle conditioned on the sampled signal. The development of the density function began with the density function conditioned on the signal and was expanded to include the case of numerous samples taken at each sensor. This was finally expanded to include the case of additive noise in the output of the sensors. The case of a linear array of sensors was presented, with the possibility of expanding the result to include two dimensional arrays of sensors.

Following the development of the density function a discussion of how the covariance is actually constructed is presented. This lead to a presentation of the algorithm used to calculate the density function given an observation vector which contains sample values of the signal at all of the sensors in the array.

Chapter 3 Discussion of Simulation and Examples of Density Functions

3.1 Introduction

In this chapter, several illustrative examples of probability density functions of bearing angle conditioned on the sampled signal data are explored. The general model for an array of sensors is given in Figure 2.

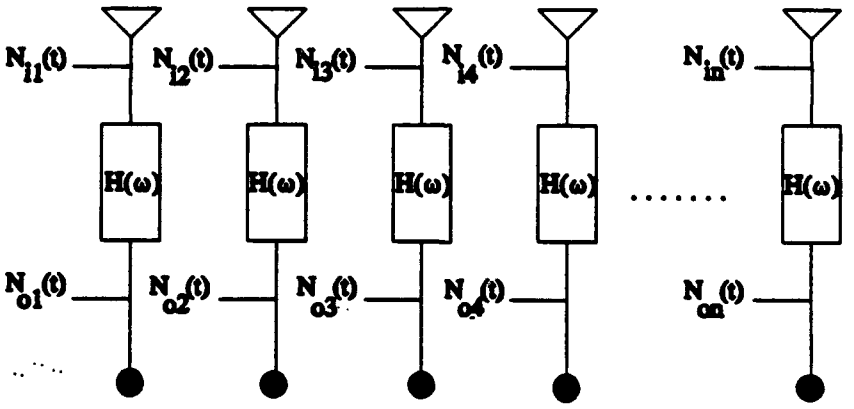

Figure 2: Model for Sensor Array

In Figure 2 a linear array of n sensors is shown. The block labeled $H(\omega)$ represents a linear filter with frequency response $H(\omega)$. This filter can be a high-pass, low-pass, or band-pass filter. The N_i's represent input noises which are uncorrelated between sensors. The N_o's represent output noises which are also uncorrelated between sensors. The examples presented in the following sections use variations on the sensor model presented in Figure 2.

For the examples given, the signal used is a narrow-band signal produced by a $MATRIX_{TM}$ simulation shown in Figure 3. The prior density function as given in Equation (18) on bearing is assumed to be uniform over the range -90° to 90°. The code which generated the following plots is given in Appendix A. First, a discussion of the simulation of the signal and noise at each of the sensors is given. This will include a presentation of the properties of a narrow band filter which is used in the sensing scheme. Following a discussion of the signal and noise simulation, a short discussion of the definition of signal-to-noise ratio is given.

Examples to be discussed will include the following. The first example is the case of an array of two sensors with one source located at different bearings in the half space in front of the array. The second example is an array of two sensors and one source where the spacing of the sensors is varied as a function of the source's center-frequency wavelength. The third example is for an array of two sensors and one source where the number of samples taken per sensor is varied. The fourth example

is for an array of two sensors where the signal to noise ratio is varied. For all of the examples except for the second, the sensor separation distance is one-fourth of the source's center-frequency wavelength.

3.2 Simulation of the Signal and Noise

It has been shown in the previous sections that the density function for the direction of arrival conditioned on the actual sensor outputs can be determined. In this section, the method employed to generate the data which is to be sampled is discussed.

A commercially available software package, MATRIXx_{TM} is employed to do the simulation. A linear system is driven with a Gaussian, uncorrelated sequence to simulate broadband noise. Further discussion of the simulation outputs is given in Section 3.4. This produces a narrow-band signal with slowly varying phase. For the examples in this section, only one linear system is used for simplicity. Many such systems can be used, however, and their outputs summed to produce a more complicated signal. For example a signal with wide-band characteristics can be used to simulate thermal or flow noise at the sensor inputs. A narrow-band signal or many narrow-band signals may also be present in the signal. These could be models for rotating machinery that is slightly out of balance. For the more simple signal used in the following examples, the frequency response of the filter can be seen in Figure 5.

The output of the narrow-band filter is split into different channels which represent the different sensors. For all of the examples discussed in this chapter, the reference sensor is represented by channel 1. The signals which go into the other channels are delayed by an amount given by Equation (1) to simulate the propagation delay between sensors. To the output of each channel, Gaussian noise is added. The noise at each sensor is made to be uncorrelated with the noise at other sensors by changing the seed in the random noise generators. A schematic for the signal and noise generators is given in Figure 3 for the case of one source and two sensors.

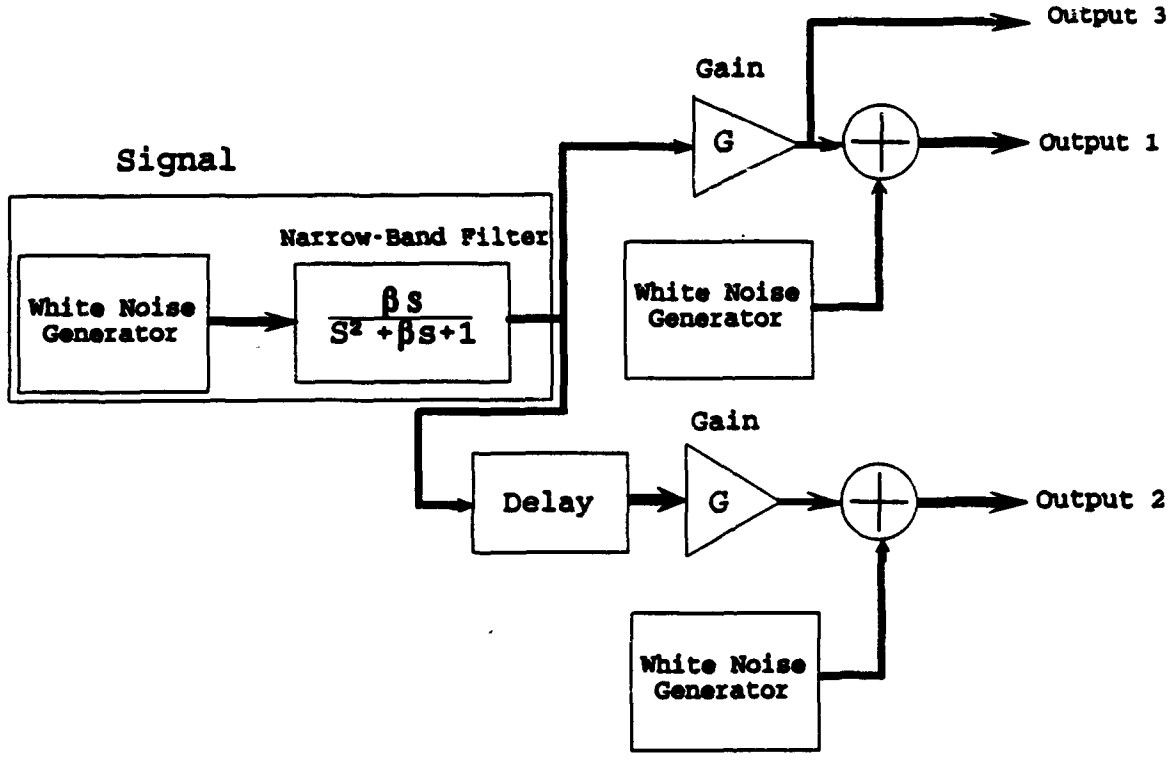

Figure 3: Schematic for Simulation of Data

The Gains G shown in Figure 3 are installed as a means of controlling the SNR. The gains are further discussed in the next section. The simulation is run for a time long enough for the signal to be uncorrelated with the initial state. The simulation in Figure 3 produces three vectors of data. The three data vectors are the signal received at the two sensors given by outputs 1 and 2 and the autocorrelation of the signal at the reference sensor which is computed after running the simulation by correlating the output 3 with itself. This is the autocorrelation of the signal at the reference sensor discussed in Section 2.5.

The outputs of the two channels are then sampled at a given sampling interval. Since the simulation produces discrete data, the data is sampled at a rate which is a multiple of the output interval. The sampled values are ordered into two data vectors which represent the data received at the two sensors. These data vectors are then combined into the signal vector given an expression similar to that of (6) except that the noise is now added. A sample of the output of the simulation from channel 1 is seen in Figure 4. The data created by the simulation are the signal, as sampled at the sensors, and the autocorrelation of the signal at the reference sensor. This data is then passed to a FORTRAN subprogram to calculate the covariance matrix discussed in Section 2.3 and the probability density conditioned on the sensor outputs.

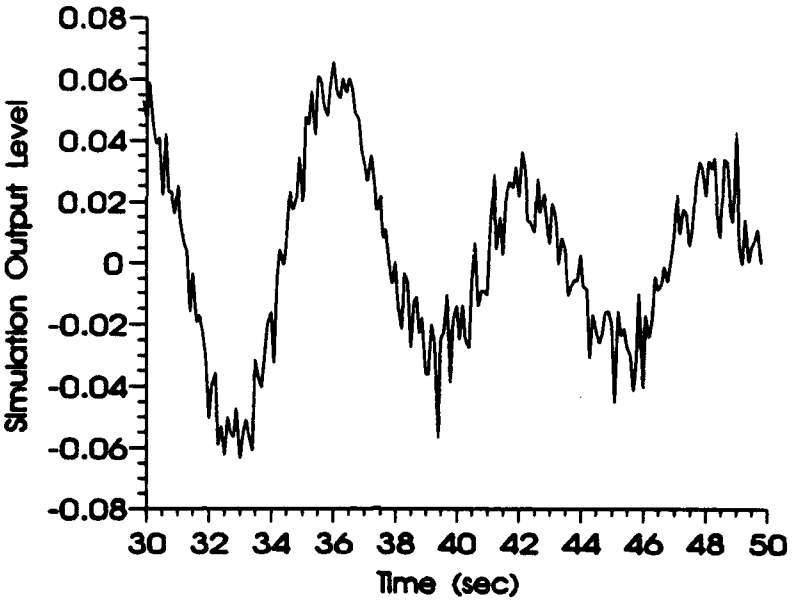

Figure 4: Output of MATRIXx Simulation for SNR=5.

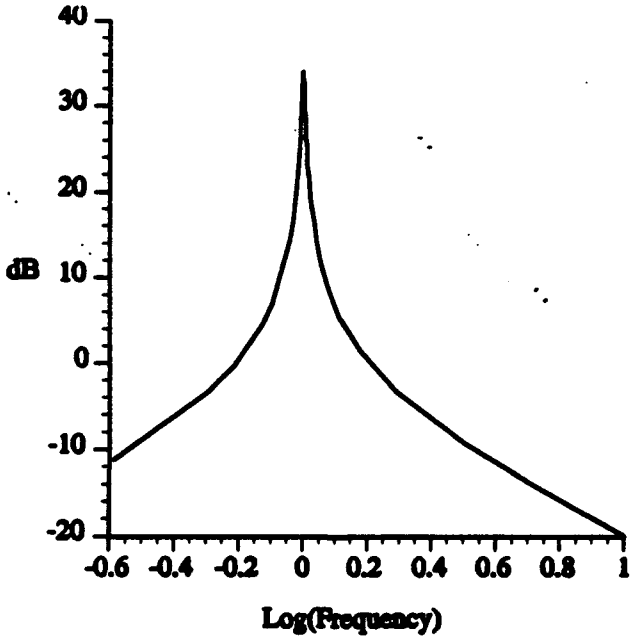

Figure 5: Frequency Response of the Filter referenced to rad/sec.

3.3 Signal-to-Noise Ratio

In this section the definition of signal-to-noise ratio is given in relation to the signal model discussed in the previous section. In particular the relation between signal-to-noise ratio and the autocorrelation of the signal and noise components of the output at channels 1 and 2.

The signal-to-noise ratio is defined as the ratio of the signal and noise variances.

$$SNR = \frac{Signal\ Variance}{Noise\ Variance} \tag{27}$$

The signal variance (σ_s^2) in (27) becomes

$$\sigma_s^2 = \int_{-\infty}^{\infty} (s-\mu_s)^2 p(s)\, ds = \psi_s^2 - \mu_s^2 \tag{28}$$

or

$$\sigma_s^2 = R_{ss}(0) - \mu_s^2 \tag{29}$$

and

$$\sigma_n^2 = R_{nn}(0) - \mu_n^2 \tag{30}$$

For the purpose of this work the signal and noise are assumed to be zero-mean and

Gaussian. The signal-to-noise ratio is therefore given by

$$SNR = \frac{R_{ss}(0)}{R_{nn}(0)} \tag{31}$$

3.4 Analysis of Simulation Outputs

In this section an analysis of the outputs on the MATRIXx™ simulation is presented. The 'whiteness' of the noise generator driving the linear system is at best questionable and criteria must be established to ensure that the noise generator appears white to the linear system. Another area to be investigated is how the signal-to-noise ratio as presented in the previous section is set in the simulation. The discussion begins with an analysis of the white noise generator.

The noise generator which drives the linear system in Figure 3 is in reality a Gaussian random number generator. The user sets the standard deviation, the seed, and the output interval. The output of the generator typically looks like the signal shown in Figure 6.

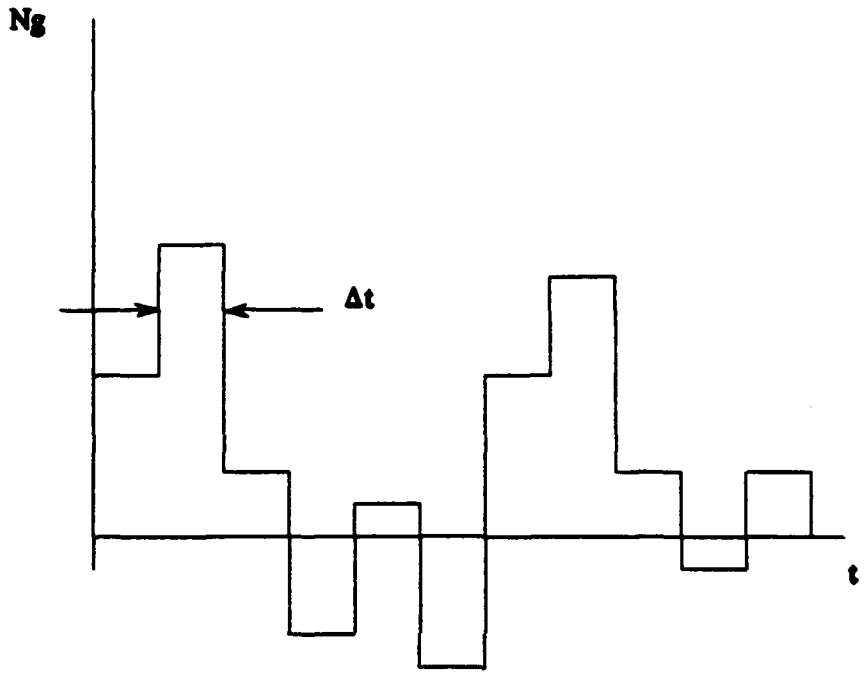

Figure 6: Output of Noise Generator

The noise generator output has an autocorrelation given by the following

$$R_{N_g N_g} = \begin{bmatrix} \frac{2\sigma_{N_g}^2}{\Delta t}\tau + \sigma_{N_g}^2 & \tau \le 0 \\ \frac{-2\sigma_{N_g}^2}{\Delta t}\tau + \sigma_{N_g}^2 & \tau > 0 \end{bmatrix} \quad (32)$$

The autocorrelation (32) looks like

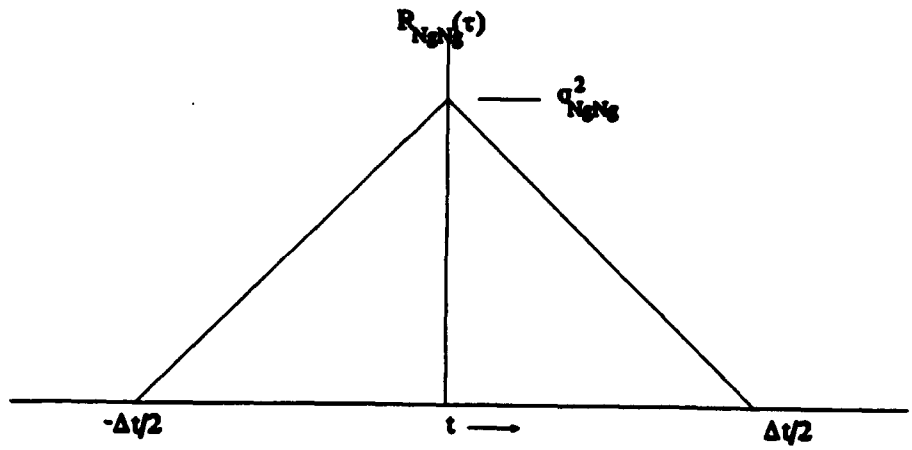

Figure 7: Autocorrelation of the Noise Sequence.

Taking the Fourier Transform of the autocorrelation $R_{N_gN_g}(\tau)$ the autospectrum $S_{N_gN_g}(\omega)$ is obtained (Bendat and Piersol, 1986, p. 121)

$$S_{N_gN_g}(\omega) = \int_{-\infty}^{\infty} R_{N_gN_g}(\tau)\, e^{-j\omega\tau}\, d\tau = \frac{\Delta t}{2}\sigma_{N_g}{}^2 sinc^2\left(\frac{\Delta t}{2}\pi\omega\right) \qquad (33)$$

This function has a main lobe the width of which is controlled by the output interval of the noise generator Δt. It is seen that by suitably choosing the value of Δt the main lobe can be made wide enough so that the spectrum at the input to the filter

appears white over some range containing the center-frequency of the filter. The criteria set for the noise signal at the input to the filter to be white is that the slope and magnitude of the autospectrum remain within 10% of the center-frequency level over twice the filter bandwidth. The filter band-width is defined as the frequency range covering the -3dB points on the frequency response curve.

The frequency response of the filter is given by the function H(s)

$$H(\omega) = \frac{j\,\omega\,\beta}{-\omega^2+\beta\,j\,\omega+1} \tag{34}$$

where β is set by the user. To see the response of the filter, the function $|H(\omega)|^2$ is plotted vs. ω in Figure 5 for a value of β set at 1.

Given the functions $|H(\omega)|^2$ and $S_{N_sN_s}(\omega)$ the power spectrum at the output of the filter is produced by the relation

$$S_{xx}(\omega) = |H(\omega)|^2 S_{N_sN_s}(\omega) \tag{35}$$

and by taking the inverse Fourier Transform of $S_{xx}(\omega)$ the autocorrelation of the output of the filter is obtained.

$$R_{xx}(\tau) = \int_{-\infty}^{\infty} S_{xx}(\omega)\, e^{-j\omega\tau} d\omega \qquad (36)$$

The autocorrelation has a maximum at a delay value $\tau=0$. By finding the maximum, the gain G in Figure 2 can be set by choosing G as the inverse of the square root of the maximum of $R_{xx}(\tau)$. This will normalize the function $R_{xx}(\tau)$ such that the maximum is set to 1.

The signal-to noise ratio is set by adjusting the standard deviation on the additive noise generators. Since the SNR is defined as the ratio of the autocorrelations of the signal and noise, respectively, and since the autocorrelation of the signal at zero delay is one, and the value of the noise autocorrelation at zero delay is the standard deviation of the noise, the SNR is given by

$$SNR = \frac{R_{SS}(0)}{R_{NN}(0)} = \frac{1}{\sigma_N^2} \qquad (37)$$

Therefore by a simple algebraic manipulation of (37) the SNR is chosen and the standard deviation of the noise generators are set accordingly.

3.5 Example 1: Effect of Change in Bearing on the Density Function

In the following example, the geometry of the array and source are as given in Figure (1). The data is produced using the simulation discussed in Section 3.2 and the probability density functions are calculated by the code given in Appendix A. The parameters which remain constant throughout the example are the number of samples per sensor $P_s=20$; the sampling interval $t_s=1$ sec; the sensor separation distance $d=\lambda/4$ where λ is the wavelength associated with the signal center frequency. A parameter which will be changed is the actual bearing angle. This is accomplished by manipulation of the delay seen in the second channel in Figure 3 which is related to the actual bearing angle by Equation (1). A plot of the probability density function conditioned on a set of sensor outputs for the above parameters, for bearings of 0^0, 20^0,45^0, 75^0 , and 85^0 is given in Figure (8). The covariances for each bearing angle for which the density is calculated are calculated off-line. The covariance is constructed using the autocorrelation of the signal at the reference sensor. The noise covariance is added to the signal covariance in the form of a diagonal matrix using (18). The main diagonal of the noise covariance contains the only non-zero values in the matrix. This occurs due to the fact that the noise is uncorrelated between sensors and with itself in time.

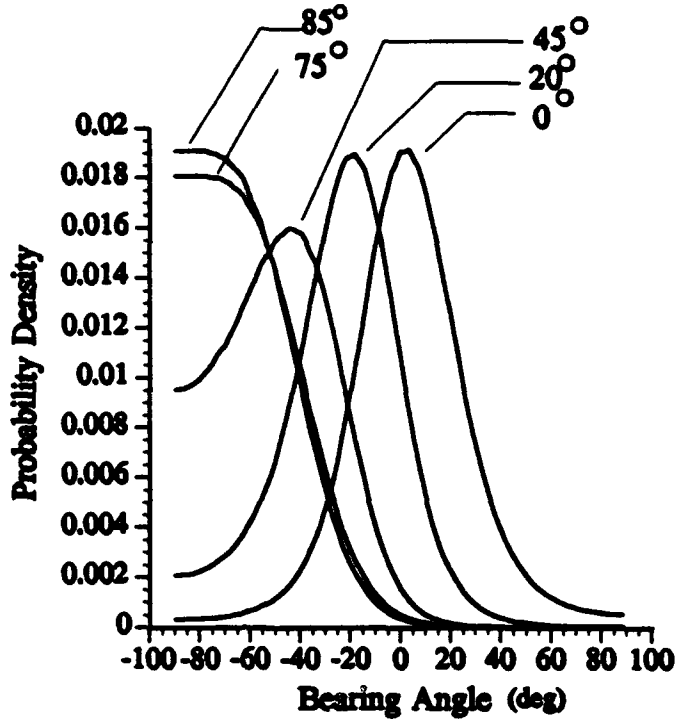

Figure 8: Probability Density Functions for Varying Bearing Angles
SNR =5, 10 Samples per Sensor at 2 sec Intervals.

The density functions seen in Figure 8 are typical examples for each given bearing. The general trends, when large numbers of density functions are generated for different data sets are shown. It is possible, however that for a given bearing, the density function can look quite different due to locally higher noise levels or a variety of other parameters. An example of varying density functions for different data sets are given in Figure 9. The densities are slightly different for each data set. This may occur due to the fact that small data sets are used and may contain locally higher or lower noise levels.

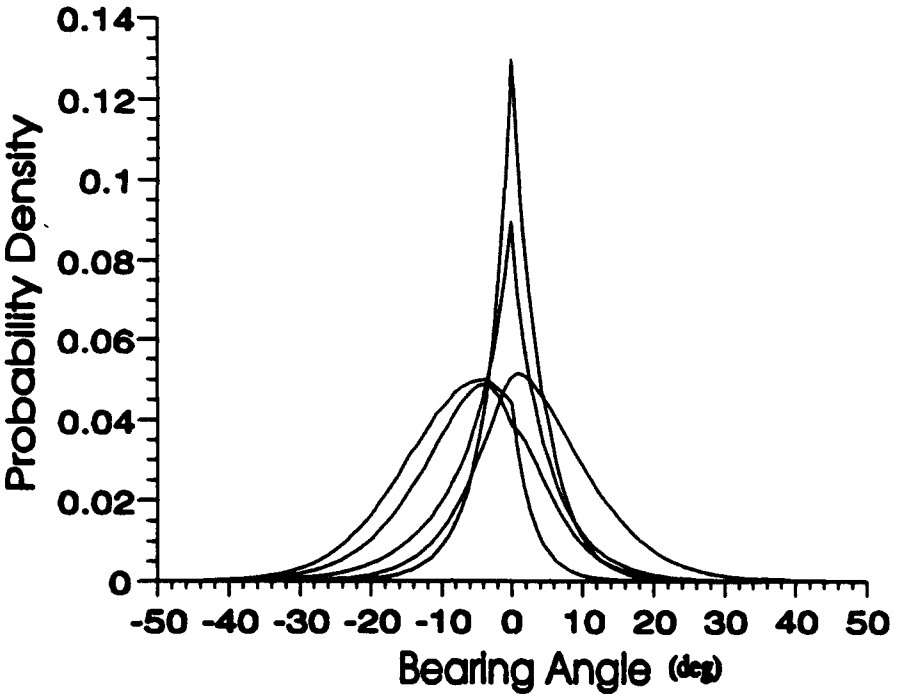

Figure 9: Varying Density Functions For Different Data Sets. SNR=5
10 Samples per Sensor at 2 Sec Intervals

The density function for zero bearing appears Gaussian. Typically, as the bearing of the source approaches $\pm 90^0$, the density functions tend to be broader with lower peaks. This indicates that less accurate estimates can be made on the bearing angle as the bearing approaches $\pm 90^0$. Very near to $\pm 90^0$ the density functions begin to narrow and the peaks tend to get higher. This occurs since the density functions are essentially "windowed" by the prior density in (18). The curves also tend to be more skewed as the bearing of the source approaches $\pm 90^0$ indicating that the disparity between the means and maximums of the densities is growing larger.

3.6 Example 2: Effect of Sensor Separation on the Density Function

In this section the effect of changing the sensor separation on the conditional density function is discussed. In Section 1.2 it was shown that the propagation delay between sensors was a function of separation distance. This relation was given by equation (1). By noting that the sound speed in the medium is given by $c=\lambda\nu=2\pi\lambda/\omega$ which gives the new form to (1)

$$\tau=\frac{2\pi d\sin(\psi)}{\lambda\omega} \tag{38}$$

In this example the distances d are chosen as a function of λ, where λ is the wavelength associated with the center-frequency of the narrow-band signal discussed in section 3.1 and ν is the center-frequency in Hz.. The distances chosen to illustrate this example are $d=\lambda/4$, $\lambda/2$, λ, and 2λ. Other parameters are the number of samples per sensor, 20, $\omega=1$ rad/sec, the sampling interval is 1 sec, and the SNR is 5. Plots of probability density functions vs. bearing angle for the above separation distances and parameters can be seen in Figures 10 and 11. It can be seen from these plots that as separation distance goes from $\lambda/4$ to $\lambda/2$, the density function becomes less broad and has a higher peak. This occurs since the aperture is effectively widened in the spatial domain. As the separation distance is widened beyond $\lambda/2$ (referred to as the Nyquist Separation from this point on) it is seen that multiple peaks occur in the density. This then appears to predict a certain amount of spatial aliasing.

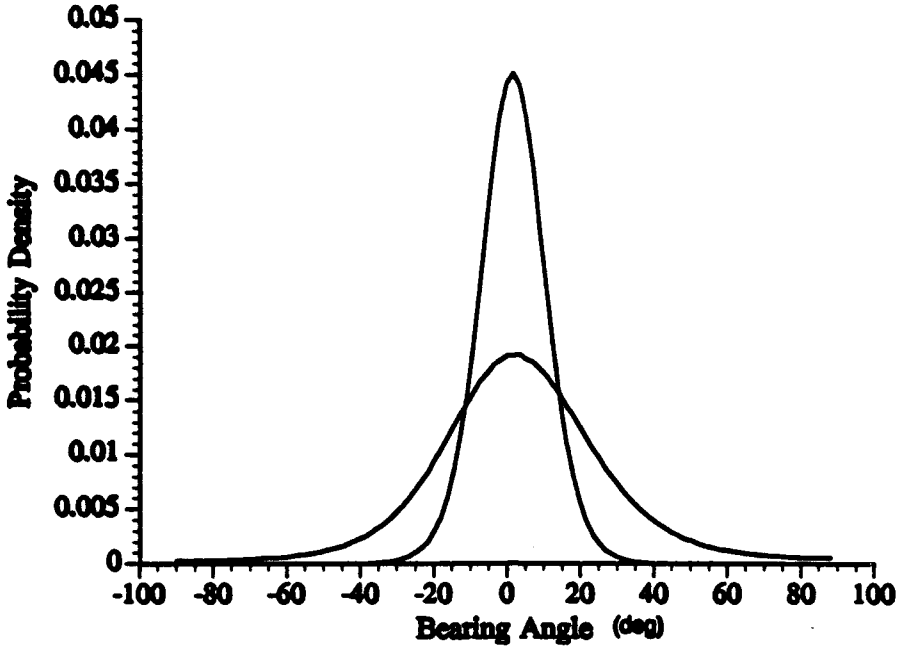

Figure 10: Probability Density vs. Bearing Angle For Varying Separation Distances SNR=5, 10 Samples per Sensor at 2 sec Intervals.

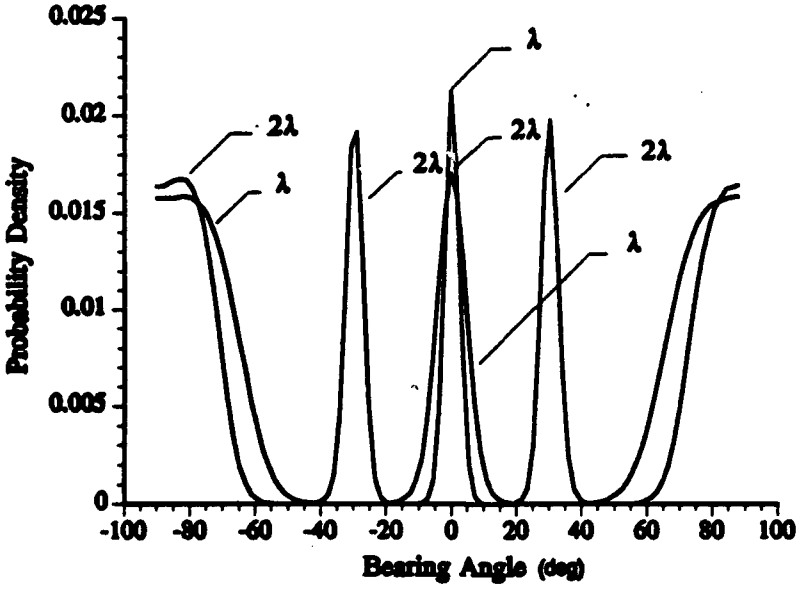

Figure 11: Probability Density vs. Bearing Angle For Varying Separation Distances SNR=5, 10 Samples per Sensor at 2 sec Intervals.

3.7 Effect Of The Number of Samples per Sensor on the Density Function

In this section, the effect of changing the number of samples per sensor is illustrated. The number of samples per sensor will be 5, 10, 15, and 20. The actual bearing of the source is 0°, the separation distance is $\lambda/4$, the sampling interval is 1 sec, and the SNR is 5. Typical density functions for the above parameters are seen in Figure 12. Again, the density functions shown reflect the general trend for a large number of density functions generated for different data sets for a given number of samples per sensor. It is possible for the density functions to have different shapes for the same number of samples per sensor. As was the case in

presented in Figure 9.

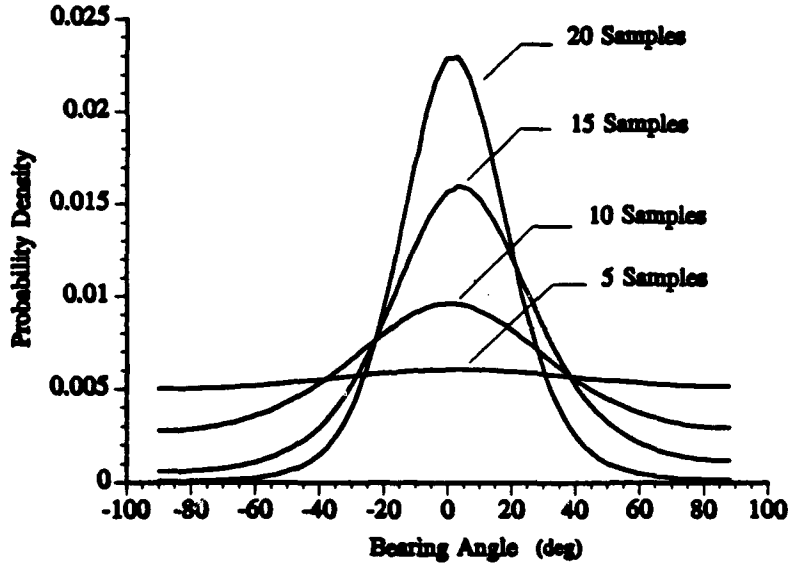

Figure 12: Density Functions For Varying Numbers of Samples per Sensor SNR=5. Sampling interval=1 sec.

As can be seen in Figure 12, the general trend is that as more samples per sensor are taken, the density function becomes more narrow and a better estimate of the actual bearing can be made. The same is true for bearings other than zero bearing, however zero bearing best illustrates the effect of changing the number of samples per sensor on the density function.

3.8 Effect of the Signal-To-Noise Ratio on the Density Function

In this section the effect of changing the signal-to-noise ratio on the density function is discussed. The signal used is the same as that used in the previous sections. In this example, the signal-to-noise ratio is varied through the values of SNR=2,5,10, and 20. The actual bearing of the source is 0°. The separation distance is $\lambda/4$ where λ is the wavelength associated with the center frequency of the narrow-band signal. The number of samples taken is 20 at a rate of 1 sample per second. The density functions for the above parameters with signal-to-noise ratios of 2,5,10, and 20 are seen in Figure 13.

The density functions shown illustrate the general trend for changes in the signal-to-noise ratio. It is possible that the density functions will take on a different shape for other data sets with all other parameters kept constant similar to the case as given in Figure 9.

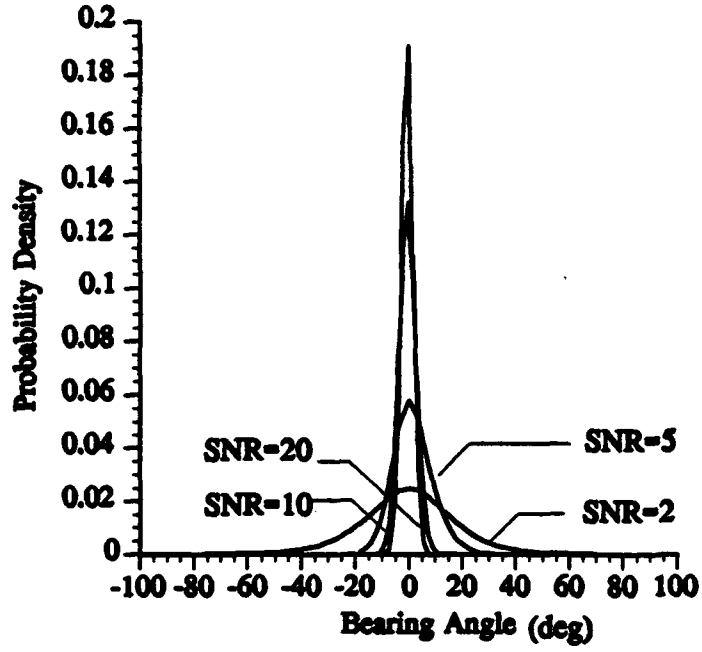

Figure 13: Density Functions for a Change in Signal-to-Noise Ratio
10 Samples per Sensor at 2 sec Intervals.

As is shown by Figure 13, the density functions become increasingly narrow as signal-to-noise ratio increases.

3.9 Summary of Results

Four illustrative examples have been explored in this chapter. The effects of changing the source bearing angle, the sensor separation distance, the number of samples taken at each sensor, and the signal-to-noise ratio have been presented. The results of these examples are summarized here.

It has been shown that as the bearing angle approaches $\pm 90^0$ the peaks of the density functions become lower and the curves become broader, making an estimate of direction of arrival less certain. Beyond this point, the peaks begin to narrow again and the curves become more narrow, however the peaks of the curves are less well defined. The peaks of the density functions become more flat, thus making an accurate estimate of bearing angle less certain.

By changing the sensor separation distance, it is shown that for a separation distance of $\lambda/4$, where λ is the wavelength associated with the center-frequency of the narrow-band signal, a single-peak well defined density function exists. When the separation distance is expanded to $\lambda/2$, the peak becomes higher and the density function curve becomes more narrow. This signifies that a better estimate of the bearing angle can be made with a wider separation distance of $\lambda/2$. This however is the widest possible sensor separation distance since beyond this distance multiple possible bearings exist. This signifies a kind of spatial aliasing analogous to aliasing experiences in digital

sampling. The separation distance of $\lambda/2$ is analogous to the Nyquist rate in digital signal processing.

For the case of changing the number of samples taken at each sensor, it is shown that as the number of samples increases, the density function becomes more narrow with a higher peak. As a result, a better estimate of the direction of arrival can be made.

By changing the signal-to-noise ratio it is shown that as the signal becomes more discernable from the noise, the density function becomes more narrow with a higher peak.

Chapter 4: The Conditional Density Function and Bearing Estimates

4.1 Introduction

In this chapter, the main focus is on the estimation of the bearing angle and other statistical properties derived from the conditional density functions. The probability density functions which are to be used in this chapter are calculated using the same methods as those in Chapter 3. The simulation which models the signal and array of sensors will be different from that in Chapter 3. In the next section, the simulation which is used will be discussed in detail. In Section 4.3, an analysis of the covariance is again presented. This is necessary since a new noise scheme is used in the simulation. Also in Section 4.3 is a discussion of some of the limitations involved in the methods used to calculate the conditional density functions. Following the discussion of the covariance, examples of density functions calculated for the new simulation are presented. In the next section, the examples mentioned above are used to complete a parametric study. In this study, such statistical properties as the maximum a posteriori estimate, the minimum mean square error estimate, and the variances on the estimates are presented. Also for a large number of densities, the means and variances of these estimates are presented with confidence intervals on the calculations. These estimate variances are compared with the Cramer-Rao lower bound for estimate variances.

4.2 Discussion of the Simulation

In this section, a discussion of the MATRIXx simulation which produces the data used in this chapter is presented. The simulation produces data for a two sensor array. The data produced by the simulation are the signal received at each sensor and the noise at each sensor. The signal is interpreted as a broadband random process which passes through the filter and becomes narrow-band. It is assumed that the noise received at each of the sensors is uncorrelated with that received at the other sensor. A schematic of the simulation is given in Figure 14.

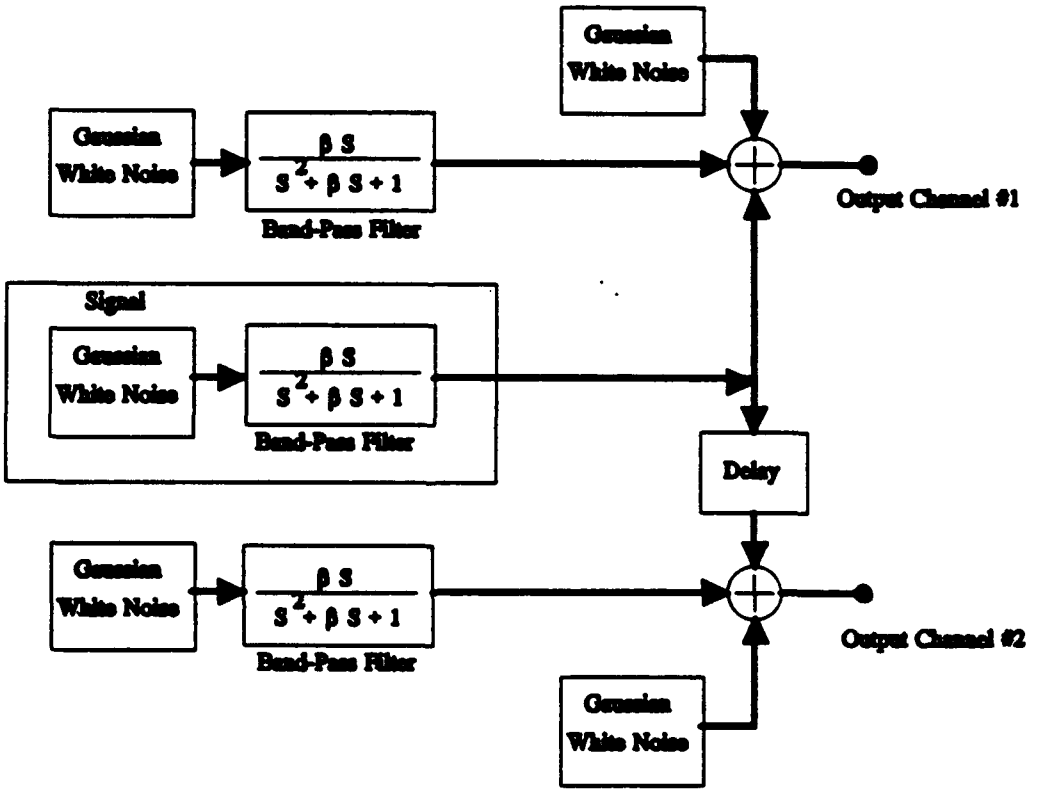

Figure 14: Schematic of Data Simulation

All of the noise sources are uncorrelated with each other. This is accomplished by setting all of the seeds in the noise generators to be different for each run of the simulation. The narrow-band filters seen in Figure 14 are the same as those used in Chapter 3. The main difference between the simulation in Chapter 3 (Figure 3) and the simulation for this chapter is that the simulation as given in Figure 14 has narrow-band noise that is uncorrelated at each of the sensors. A physical example of this would be flow noise which is passed through a narrow band filter. As in the simulation in Chapter 3, the noise spectrum is sufficiently broad compared to the band-width of the filter that it can be assumed white. The noise sources which appear after the filter are also broad-band random noise sources which can be interpreted physically as electrical noise. In all of the simulation runs, the electrical noise is set to be considerably lower than that of the noise found external to the sensor. This assures that the covariance will not be singular by adding a diagonal component.

In the construction of the covariance the narrow-band noises appear as block diagonal elements. There is no correlation of the noises between sensors. This implies that the inter-element cross-terms in the covariance will all be zero. The autocorrelation of the noise at each sensor has a non-zero value. Since the broad-band noise is modeled as white, the electrical noise contributes only to the main diagonal of the covariance matrix (i.e. each sample is only correlated with itself). Further discussion of the covariance matrix appears in the next section.

There now exist two noise sources. The signal-to-noise ratio will now be defined as the ratio of the sum of the variances of the noises to the variance of the signal.

4.3 Discussion of the Covariance Matrix

In this section, the changes which occur in the covariance matrix are discussed. As mentioned above the main difference is that there are now block diagonal elements in the covariance due to the filtered noise. Since the signal and noise both pass through the same filter, and since both are broad-band processes, the autocorrelations of the signal and noise will have autocorrelation functions which have the same shape, but have different levels. That is, the noise autocorrelation is a multiple of the signal autocorrelation. Since the noise processes are uncorrelated between sensors, the noises show up in the covariance as a block diagonal matrix added to the covariance of the signal alone. That is, the noise covariance which appears in (18) is a block diagonal matrix where the subblocks which appear above and below the main diagonal contain only zeroes. The main diagonal of the covariance matrix is the sum of the value of the autocorrelation of the signal at zero, the variance of the broad-band noise, and the variance of the narrow-band noise.

Another important point to make about the covariance matrix is that near singularities occur for various bearing angles. The number and frequency of near singularities can be related directly to the number of samples taken at each sensor, the sampling

interval, and the spacing between sensors. The near singularities occur for bearings which have a propagation time delay between sensors (τ) which is equal to the sampling interval and integer multiples of the sampling interval. Figure 15 illustrates this using one period of a cosine wave as the autocorrelation. The symbols , x, represent the values of the autocorrelation of the signal at the reference sensor with later samples at the reference sensor. The symbols, □, represent the correlation between the samples at the reference sensor and the samples at a second sensor. As dt, the sampling interval, approaches the magnitude of the propagation delay, τ, the near singularities occur (i.e. when the x's and the □'s overlap). This happens since the elements in the covariance off-diagonal subblocks are shifted versions of the diagonal subblocks. When this occurs, the covariance in near singular. It has been shown that the least number of near-singularities occur when the sampling interval corresponds to the Nyquist sampling interval corresponding to the center frequency of the signal. Also the spacing should be near the spacing corresponding to a half wavelength of the center frequency of the signal.

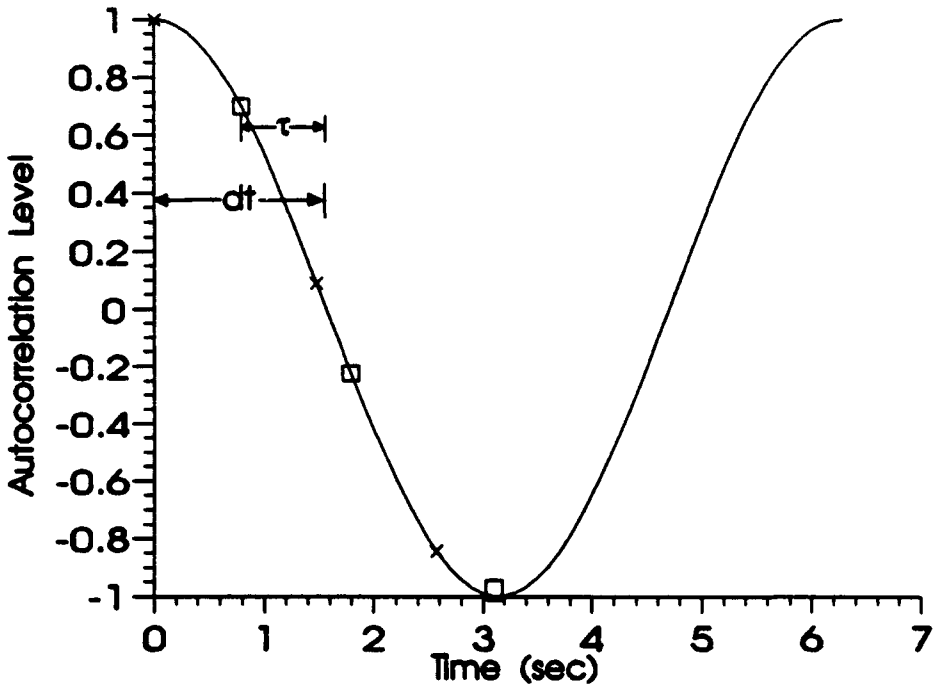

Figure 15: Sampling Interval, Propagation Delay, and Covariance Singularities

In order to illustrate the effect of covariance singularity, the condition number of the matrix is plotted as a function of bearing angle. The condition number is defined as the ratio of the largest to the smallest eigenvalues of the covariance. The larger the condition number, the closer to singular the covariance matrix. Figure 16 shows the condition number as a function of bearing.

Figure 16 shows plots of the condition number as a function of bearing angle for three sampling schemes. The lowest curve is for Nyquist sampling which is 10

samples/sensor at 2 sec intervals. The middle curve is the condition number plot for 20 samples per sensor at a 1 sec sampling interval. The bearing which corresponds to the 1 sec sampling interval is $\pm 39.5°$(this is found using Equation 1). It is seen that the peak does in fact occur at -39.5°. The highest curve is for over-sampling with 20 samples/sensor at 0.5 sec intervals. The peaks should and do occur at the points $\pm 18.6°$, $\pm 39.5°$, and $\pm 72.7°$ which correspond (through Equation 1) with the 0.5, 1, and 1.5 sec delays. It is also seen that all of the sampling schemes have near-singularities at 0°.

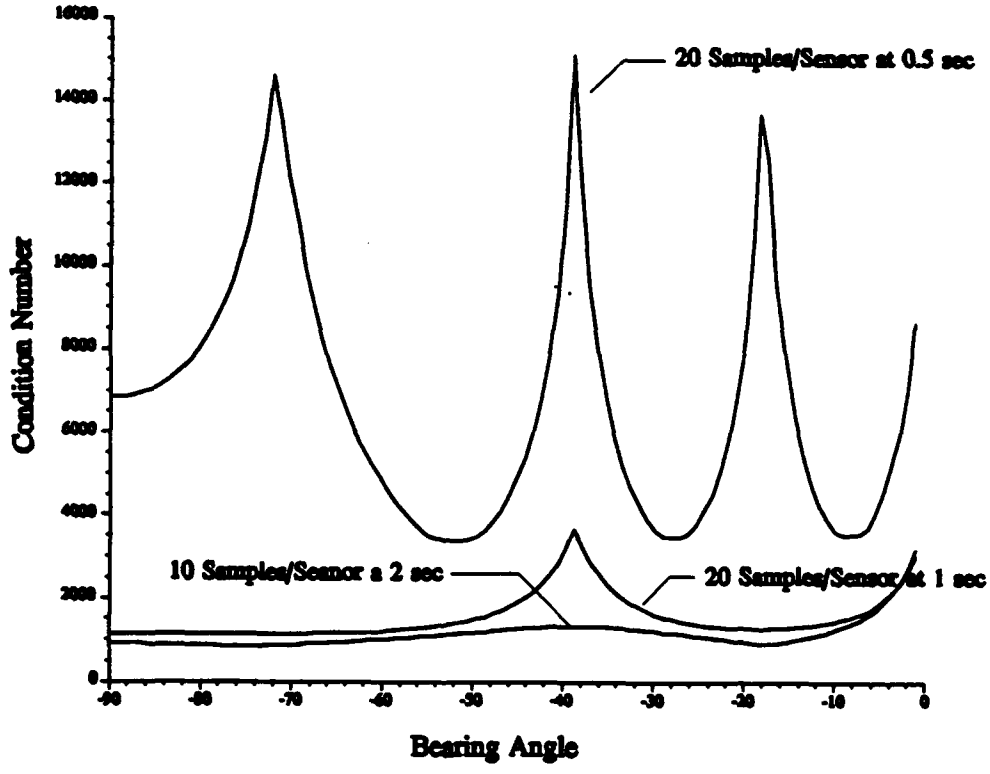

Figure 16: Condition Number of Covariance vs. Bearing Angle

4.4 Estimation of Bearing Angle

In this section the methods of estimation of bearing angle are discussed. The two methods used in the estimation of bearing are the minimum mean square error (MMSE) estimate and the maximum a posteriori estimate (MAP). The data used in the calculation of the density functions used in the calculations to follow is produced by the simulation discussed in Section 4.2.

The first method of estimation that is considered is the minimum mean square error method. The density function for bearing is calculated for source bearings ranging from 0° to 90°. For each bearing, the density is calculated for each of 400 data sets randomly selected from a large simulated data set. For each of these 400 density functions the mean is calculated using:

$$\mu_\psi = \int_{-\infty}^{\infty} \psi \, p_{\psi|Y}(\psi|Y)\, d\psi \approx \sum_{i=1}^{P_a} \psi_i p_{\psi_i|Y}(\psi_i|Y)\, \Delta\psi \tag{39}$$

The means which are calculated from (1) for each data set are then averaged over all data sets to arrive at the average estimate of bearing.

$$MMSE = \frac{1}{ds} \sum_{j=1}^{ds} \mu_j \tag{40}$$

where ds is the number of data sets.

The second method employed is the MAP estimate. In this method the same 400 data sets are used to calculate the densities. In this method the estimate is made by choosing the angle which corresponds to the largest value of the density. A maximum is found for each of the 400 density functions and the corresponding estimates of angle are averaged to arrive at the average MAP estimate.

$$MAP = \frac{1}{ds} \sum_{j=1}^{ds} Max_j \tag{41}$$

where Max_j is the maximum density for the j'th data set. Again, ds is the number of data sets.

Figures 17, 18, and 19 plot the MMSE and MAP estimates as a function of actual bearing angle for various sampling schemes. Figure 17 gives the estimates for a sampling scheme of 10 samples/sensor at 1 sec. intervals. Figure 18 gives the estimates for a sampling scheme of 20 samples/sensor at 1 sec. intervals. Figure 19 gives the estimates for a sampling scheme of 20 samples/sensor at 0.5 sec. intervals. The sensor separation for all examples is $\lambda/4$. The SNR is 5. The confidence intervals shown in Figures 17 through 22 have 90% coverage (see Appendix b).

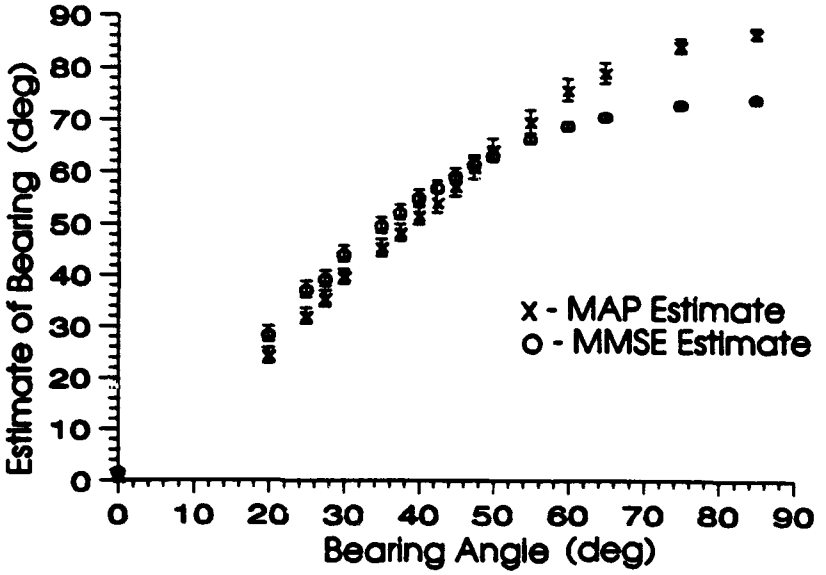

Figure 17: Estimate vs. Actual Bearing(10 Samples/ Sensor - 2 sec Interval) SNR=5.

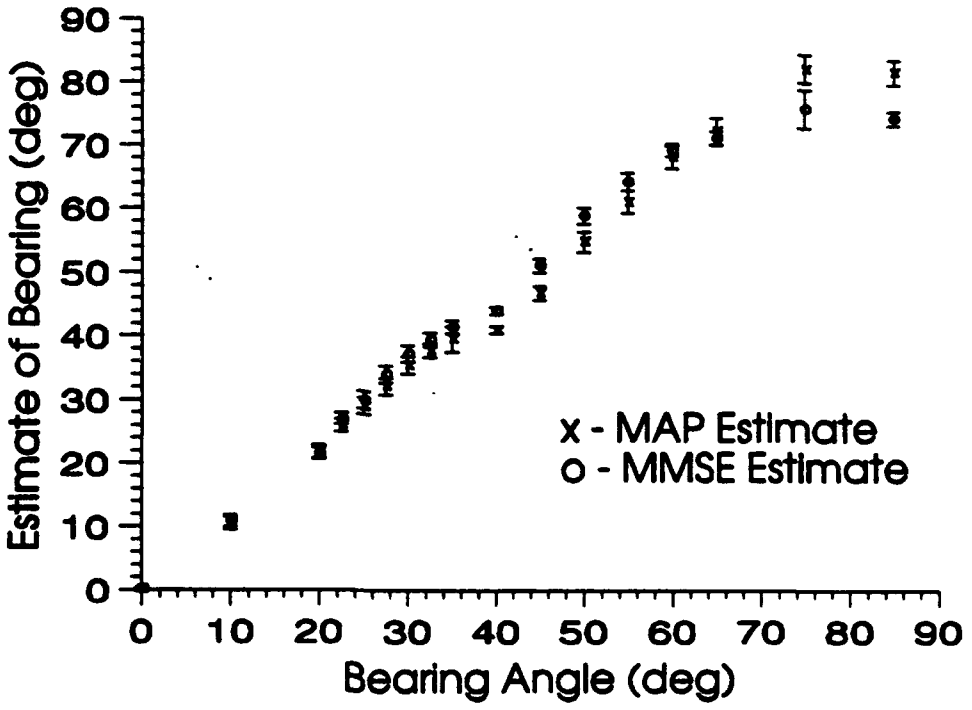

Figure 18: Estimate vs. Actual Bearing (20 Samples/Sensor 1 sec Interval) SNR=5.

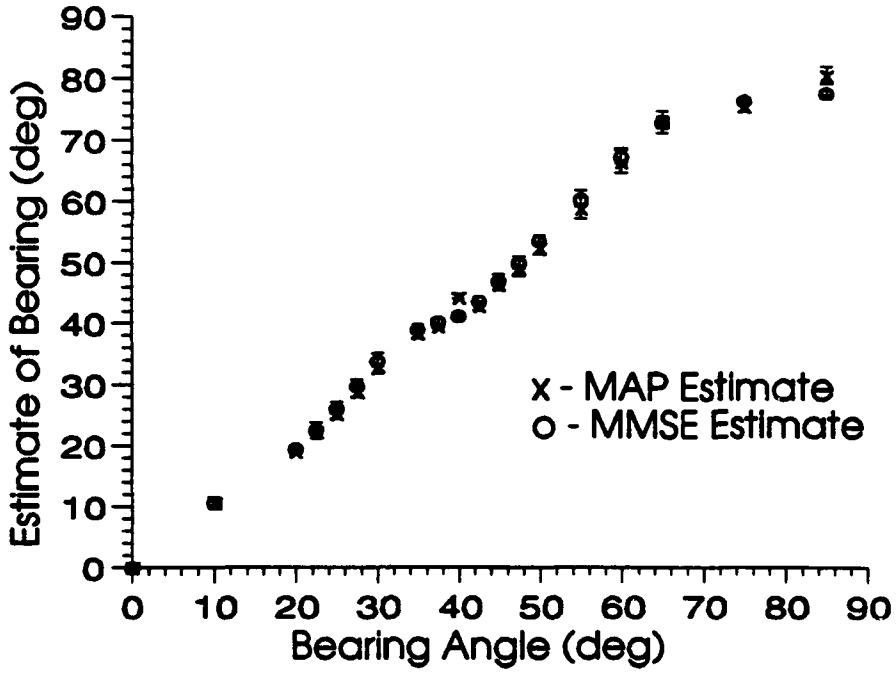

Figure 19: Estimate vs. Actual Bearing (20 Samples/Sensor 0.5 sec Interval) SNR=5.

It is seen that as the number of samples increases, the estimates of bearing more closely reflect the actual bearing. This is also true for the case of increasing the resolution of the sampling as in Figure 19. In all cases the estimates cross each other in the 50° - 60° range. This indicates that the density functions become skewed as the actual bearing approaches $\pm 90°$. The meaning of 'skewed' is that the mean value of the density function and the angle which corresponds to maximum value of the density function are not the same. The fact that the MMSE estimates become lower than the MAPs indicates that the mean values of bearing are on average lower than the values

of bearing for which the density is a maximum. This then is the statistical support of the observation that the densities become skewed as bearing angle approaches $\pm 90^{\circ}$ made in Section 3.5. To better understand these trends is necessary to look at more statistics derived from the density functions.

4.5 Statistics on the Estimates

In this section, the statistics of the estimates are presented. In the last section, the average estimates of bearing are calculated using a large number of data sets to calculate the conditional probability density function for each data set. Using the same techniques as in the previous section, the variance of the estimates is calculated. The variances of the MAP and MMSE estimates are plotted as a function of bearing together with the Cramer-Rao bound on the variances. The statistics are different because the assumptions about the bearing made in the thesis are fundamentally different from those made in the derivation of the Cramer-Rao bound (C-R Bound). The C-R bound assumes that sufficient prior information in known about the bearing so that the covariance of the data is known. Under this assumption, the density $p_{Y|\psi}$ is Gaussian, and both the MAP and MMSE estimates are identical. When the bearing can be resolved with sufficient accuracy that the covariance matrix can be assumed constant over the region for which $p_{\psi|Y}$ is non-trivial, the C-R bound accurately reflects the performance of the Bayes optimal estimators. When the variations of the covariance matrix cannot be ignored (as happens at low SNR) the C-R bound does

not reflect the likely performance of the optimal estimators. It is important to note that under the assumptions used to derive the optimal MAP and MMSE estimators, the former estimate is not unbiased, and neither is consistent, therefore both may have variances lower than the C-R bound.

The Cramer-Rao bound is the lower bound on the estimate variance and is given by the relation

$$Var[\psi(R)-\psi] \geq \left(-E\left[\frac{\partial^2 \ln(p_{Y|\psi}(Y|\psi))}{\partial \psi^2} \right] \right)^{-1} \tag{42}$$

where ψ is the estimate of the real non-random parameter ψ and $p_{Y|\psi}(Y|\psi)$ is the conditional probability density function of the data r conditioned on the real variable ψ.

The calculation of the Cramer-Rao bound is as follows.

The logarithm of the density function (4) is taken

$$\ln(p_{Y|\psi}(Y|\psi) = -\ln((2\pi)^{\frac{m}{2}}|R_{YY}|^{\frac{1}{2}}) - \frac{1}{2} Y^T R_Y^{-1} Y \tag{43}$$

The second derivative with respect to ψ is taken

$$\frac{\partial^2}{\partial \psi^2} \ln(p_{\eta|\psi}(Y|\psi) = -\frac{\partial^2}{\partial \psi^2} \ln((2\pi^{\frac{M}{2}}|R_Y|^{\frac{1}{2}}) - \frac{\partial^2}{\partial \psi^2}(\frac{1}{2} Y^T R_Y^{-1} Y) \tag{44}$$

The second derivative is found by fitting a second order polynomial to (43) near and including the point at which the second derivative is to be calculated. This is accomplished by first finding the interpolating polynomials given by

$$l_i(\psi) = \prod_{j=1, j\neq i}^{3} \frac{\psi - \psi_j}{\psi_i - \psi_j} \quad i=1,2,3 \tag{45}$$

The l_i's are second order polynomials. The interpolation requires three points: the point at which the derivative is to be calculated and two points close to either side. The interpolation function is given by

$$x(t) = \sum_{k=0}^{2} x_k l_k(\psi) \tag{46}$$

where the X_k's are coefficients to the polynomials given by the functions $\ln((2\pi)^{(m/2)}|R_Y|^{1/2})$ and $(\frac{1}{2} Y^T R_Y^{-1} Y)$ evaluated at the three points ψ_1, ψ_2, and ψ_3.

The second derivative for a second order polynomial is given by the following

$$\frac{\partial^2}{\partial \psi^2} X(\psi) = \frac{2x_1 \psi}{(\psi_1 - \psi_2)(\psi_1 - \psi_3)} + \frac{2x_2 \psi}{(\psi_2 - \psi_1)(\psi_2 - \psi_3)} + \frac{2x_3 \psi}{(\psi_3 - \psi_1)(\psi_3 - \psi_2)} \tag{47}$$

The Cramer-Rao bound is found by taking the inverse of the expectation of the relation (43).

$$\sigma_{CR}^2 = \frac{1}{E[\frac{\partial^2}{\partial \psi^2}\ln((2\pi)^{\frac{m}{2}}|R_Y|^{\frac{1}{2}})] + \frac{1}{2}E[\frac{\partial^2}{\partial \psi^2}Y^T|R_Y|^{-1}Y]} \tag{48}$$

The expectation of the first term of (43) is a scalar. Finding the expectation of the second term is more involved. The second derivative operator is moved to the inverse of the covariance giving

$$R'' = \frac{\partial^2}{\partial \psi^2} R_Y^{-1} \tag{49}$$

R" can be represented by a singular value decomposition by

$$\therefore R'' = U\Sigma U^T = Q^T Q \rightarrow Q = \Sigma^{\frac{1}{2}} U^T \tag{50}$$

A new variable is defined as Z=QY. Using this new variable the relation for the expected value of the second term on the right hand side of (43) can be rewritten

$$E[Y^T R'' Y] = E[Y^T Q^T Q Y] = E[Z^T Z] = Trace[E[Z Z^T]] \tag{51}$$

by replacing Z with the proper values (51) can be reduced to

$$E[Y^T R'' Y] = Trace[E[Q Y Y^T Q^T]] = Trace[Q\, E[Y Y^T] Q^T] \tag{52}$$

The term on the far right of the (52) contains the term E[Y Y^T]. This is simply the covariance of the data. Therefore, the entire Cramer-Rao bound can be written as

$$\sigma^2_{CR} = \frac{1}{-\frac{\partial^2}{\partial \psi^2} \ln((2\pi)^{\frac{m}{2}} |R_Y|^{\frac{1}{2}}) - \frac{1}{2} Trace[Q R_{YY} Q^T]} \tag{53}$$

where the derivatives are calculated as mentioned above for the calculations of the first term on the right hand side and to find the value of Q. It is important to note that (53) is for unbiased estimators. In our case the variable is bearing angle. Note that the density function appearing in (4) is not the density calculated in the previous sections. The C-R bound is interpreted as the lower bound on the variance of the estimate based on the probability density of the data conditioned on the bearing angle. It is important to keep in mind that the density function calculated in all of the MMSE and MAP estimates is the density function of the bearing angle conditioned on the actual data. One then sees that the C-R bound on the variance is arrived at by assuming that the source is in a given direction and then based on the data gives a

lower bound on the estimate variance. The MAP and MMSE estimates are made based on the assumption that the data is reflective of a certain bearing angle. In other words the C-R bound assumes the source is in a given direction then sees how close the data reflects that bearing. The method used to calculate the variance of the estimates in the MAP and MMSE estimates make no assumption of bearing angle except that the prior density on bearing is uniformly distributed. The estimates are made on the directly calculated probability density of bearing angle based on the actual data. The question is then what is the relationship between the C-R bound and the variance of the estimates using our calculated density functions. This question needs to be asked so that the comparison of a relatively well known lower bound, the C-R bound, and the variances of the estimates made using the directly calculated density functions can be made. The answer to this is that the C-R bound shows what kind of results are obtained using an efficient estimator such as a maximum likelihood estimator using the known covariance of the data. Figures 20, 21, and 22 show the MAP and MMSE estimate variances along with the C-R bound.

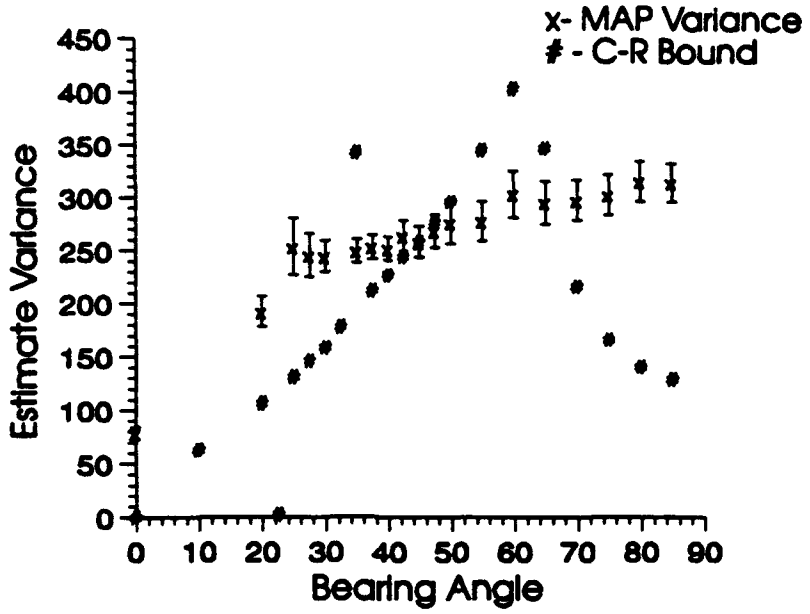

Figure 20a: Estimate Variance vs. Bearing (10 samples/Sensor 2 sec Interval)

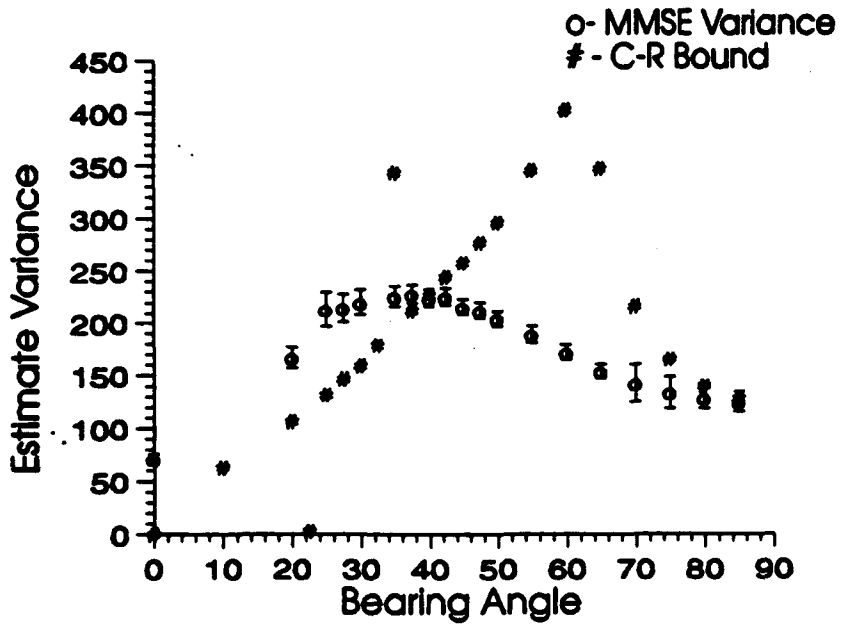

Figure 20b: Estimate Variance vs. Bearing (10 samples/Sensor 2 sec Interval)

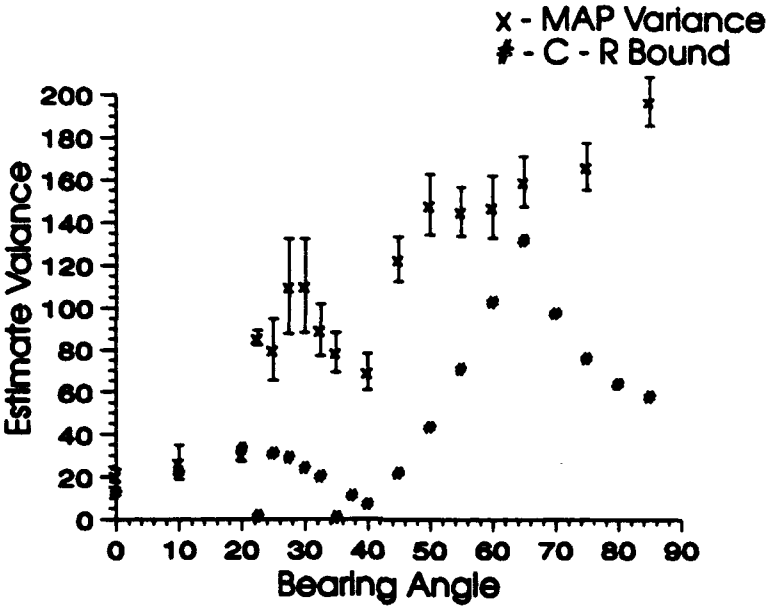

Figure 21a: Estimate Variance vs. Bearing (20 Samples/Sensor 1 sec Interval)

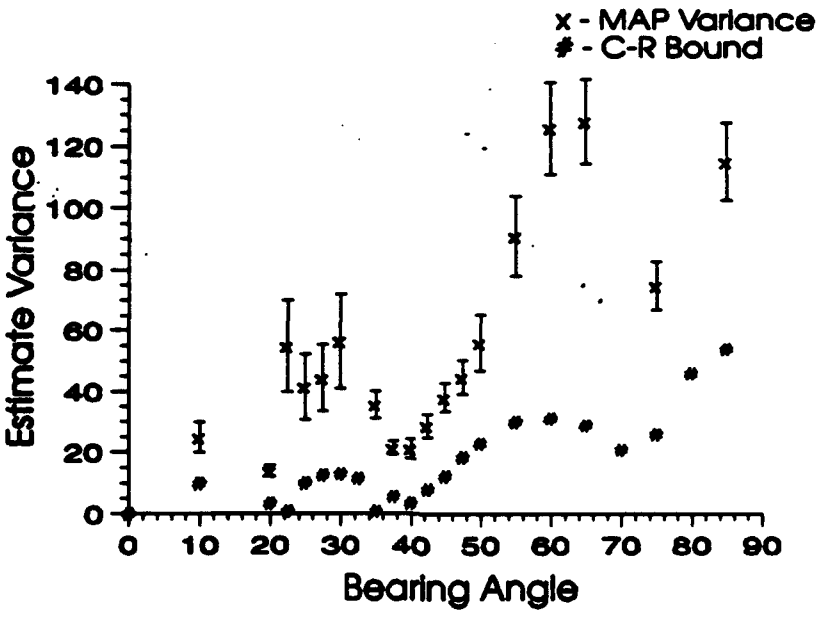

Figure 21b: Estimate Variance vs. Bearing (20 Samples/Sensor 1 sec Interval)

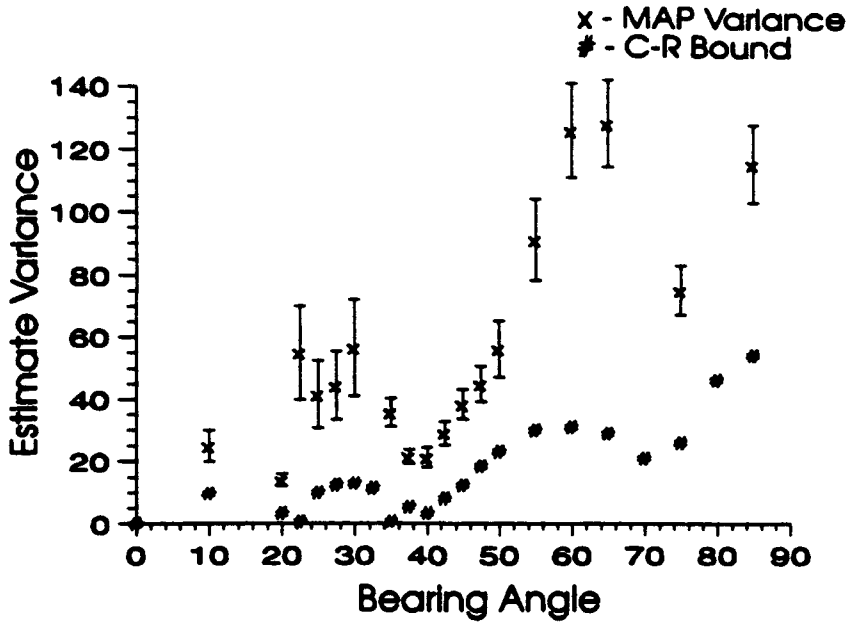

Figure 22a: Estimate Variance vs. Bearing (20 Samples/Sensor 0.5 sec Interval)

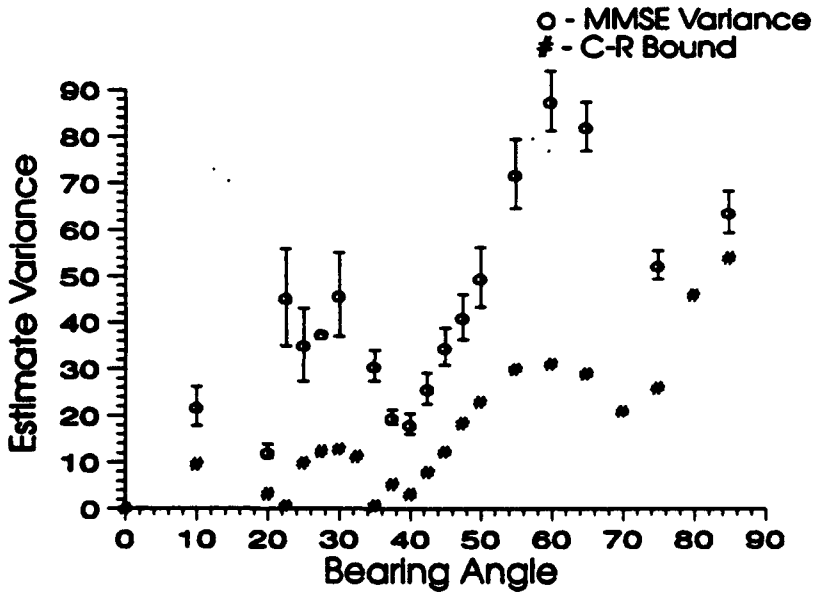

Figure 22b: Estimate Variance vs. Bearing (20 Samples/Sensor 0.5 sec Interval)

The first trend that is seen is that as the number of samples increases or if the sampling resolution increases, the C-R bounds get lower. It is also seen that in the 10 sample case the highest variance (worst estimate) is at a bearing angle of approximately 65°. This is an unexpected result. One would expect that as the actual bearing approached ±90° the variance of the estimate would increase steadily. To better understand why this occurs one has to look at the averaged density functions. An average density function is the average of the density functions which have been calculated for a number of data sets. Figure 23 is a plot of the averaged density functions for 400 data sets. One sees that as the curves approach the -65° bearing angle, the densities are the flattest and the widest. This makes the estimation of bearing difficult to make hence the largest variance on the estimate. As the curves move past the ±65° bearing, the curves become sharper with higher peaks. This occurs due to the fact that the density functions are windowed (in the range ±90°) by the uniform distribution in Equation (18). Since the curves have higher peaks and are narrower, the variance on the estimates will be lower in this range and continue to get lower as the actual bearing of the source approaches ±90°.

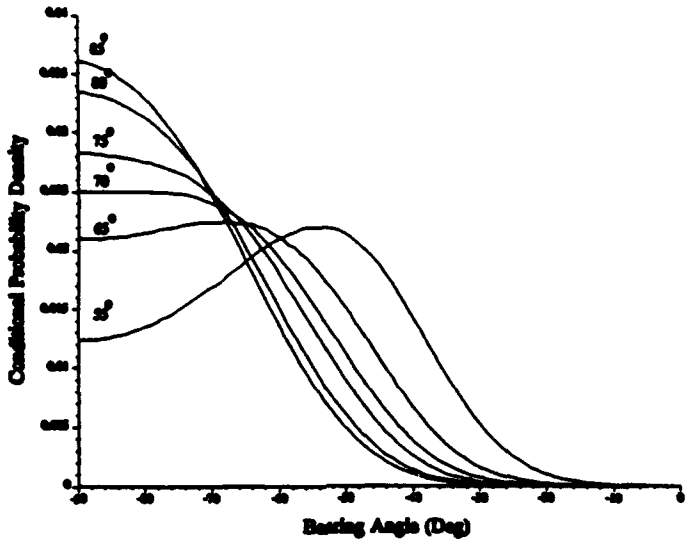

Figure 23: Averaged Density Functions (10 Samples/Sensor 2 Sec Interval)

It is also seen that low points or "dips" occur in the C-R curves for certain sampling schemes and certain bearings. These values are the same as those discussed in section 4.3 for which the condition number peaks. It is at the values which the covariance matrix becomes near singular that the variances have smaller values. By comparing Figures 20, 21, and 22 it is seen that the near singularities corresponding the sampling interval have a definite effect on the variances of the estimates. For example, the near singularity which occurs at 70° in Figure 22 for a sampling scheme of 20 samples /second at 0.5 second intervals, brings the peak in the variance curve at 65° down. The trend, therefore, in this particular sampling scheme more closely resembles the expected trend that the variance of the estimates of bearing goes up as

bearing angle approaches $\pm 90°$.

Looking at the sampling schemes and how they affect the variances on the estimates is also interesting. As seen in Figure 20 the MMSE and MAP variances are smaller than the C-R bound for bearings greater than approximately 40° and for the MAP estimate for bearings less than 70°. This is true only for the case of the nyquist sampling. The MMSE is the lowest with the trend being that there is a peak occurring around 30° and then the variances drop off as the bearing angle approaches 90°. The second sampling scheme, where 20 samples per sensor are taken at 1 sec. intervals is seen in Figure 21. The immediate observation is that the variance curves have low points in them at approximately 40°. This is the point at which the condition number of the covariance is large as seen in Figure 16. Since the variance here is the lowest, the best estimates of bearing can be made here. It is also noticed that for this particular sampling scheme, the variances are all closer together. The MMSE is still generally lower than the MAP and C-R bound, but the C-R bound is now clearly lower than the MAP estimate variance curve. Notice that a peak still exists in the C-R curve at approximately 65°. The reasons for this are that same as those discussed above for the 10 sample per sensor case. Finally, looking at the 20 samples per sensor case at 0.5 second intervals, the correlation between the condition number of the covariance matrix and the variance plots is really apparent. All of the estimate variance curves in Figure 22 have low points at approximately 20°, 40° and 70° bearings. Looking back we see in Figure 16 that the condition number plot for

this sampling scheme has peaks at precisely these points. Therefore better estimates can be made for a sampling schemes with more samples per sensor with shorter intervals between samples. This is true due to the fact that not only are the curves generally lower, but singularities occur in the covariance matrix for more bearing angles which in turn causes more low points in the estimate variance curves.

4.6 Summary and Conclusions

In this chapter a new simulation was created with a more complicated noise model. The effect of this new data model on the covariance matrix of the data is discussed and the net effect is found to be that block diagonal components which are a multiple of the signal blocks are added to the covariance. This is true since the noises at each sensor are correlated with themselves, but are assumed to have zero cross-correlation between sensors.

Using the new simulation, new data is created which is used to calculate the probability density functions conditioned on this data. The density functions are calculated for a number of examples using various sampling schemes on the data. The density functions are then used to make estimates on the actual bearing angle. Two types of estimates are made. The first is the minimum mean square error

estimate (MMSE). The second is the maximum a posteriori estimate (MAP). It is found that as the number of samples is increased, or if the sampling interval is shortened, the estimates more closely reflect the actual bearing.

A measure of how accurate the estimates are is then discusses in the form of the variances on the estimates. A known measure of performance is then introduced: the Cramer-Rao bound (C-R). The C-R bound gives the lower bound on the variance of estimates given by an unbiased estimator. The variances on the MAP and MMSE estimates are lower than the C-R bound for Nyquist time and spatial sampling, but the C-R bound is lower for any form of over sampling.

Another trend is found in relation to the variances on the estimates and the condition number of the covariance matrix. The sampling schemes which have over-sampling contain low points in the estimate variance curves which correspond to bearings where the covariance has high condition numbers (covariance matrix approaching singularity). For Nyquist sampling, there are no singularities except at 0^0 bearing. As the sampling interval or number of samples is significantly increased, the number of bearings at which the covariance is singular will increase and the variances on the estimates will be lower which indicates that better estimates on the actual bearing can be made.

Chapter 5: Summary and Conclusions

5.1 Introduction

In this chapter the results obtained in the thesis are discussed. The general outline of the chapter will follow the outline of the thesis giving the results obtained thought. The results section will give a brief description of the goals for major topics in the thesis. The opening discussion of a general topic is followed by the results which are presented in the thesis and how well the goals of the section are fulfilled. The chapter ends with a section which is dedicated to recommendations for further research.

5.2 Conclusions and Results

In Chapter 2 the derivation of the probability density function conditioned on the sensor inputs is presented. It is shown that the conditional density function is calculated by first calculating the probability density function of the data conditioned on the bearing angle. This density function is used in Bayes' formula to calculate the probability density function of the bearing angle conditioned on the sampled data.

Following the derivation of the probability density function, an analysis of the covariance matrix of the data is presented. This analysis begins with the placement of the data into an ordered vector which is multiplied by its transpose. The expected value of this product is then taken to give the covariance. Following this discussion, the code which is used to generate the covariance is discussed is detail.

In Chapter 3, a simulation used to generate some of the data used in the thesis is presented. The elements of the simulation ore discussed, and criteria are set to insure that the outputs reflect the sensor model. The outputs of the simulation are analyzed in order to give meaning to definitions of signal-to-noise ratio and the 'whiteness' of the noise processes.

The next part of the thesis, also in Chapter 3, are four sections each devoted to a different example. Each section contains an example in which various parameters are changed. The parameters changed are the bearing angle, the sensor separation distance, the number of samples taken at each sensor, and the signal-to-noise ratio. In the first example it is found that as bearing angle approaches $\pm 90°$, the density functions become broader and have lower peaks. This occurs up to a point at which the densities begin to narrow and have wider peaks. This is due to the fact that the densities are cut off at $\pm 90°$. The second example shows that as the sensor separation distance is increased, the number of possible bearings also increases. This is due to spatial aliasing. The separation distance is larger that the half-wavelength of

the center-frequency of the signal causing a sort of aliasing. The optimum distance where no aliasing occurs is the Nyquist separation distance where the separation distance is half the wavelength of the signal center frequency. In the third example it is shown that as the number of samples increases, the density curves become more narrow with higher peaks. The result is that with more samples, a better estimate of bearing angle is achieved. The fourth example, where the signal-to-noise ratio is changed, shows that as the signal-to-noise ratio is increased, the curves become more narrow with higher peaks. This also shows that as the SNR is increased, better estimates of bearing can be made.

In Chapter 4, a modification of the simulation discussed in Chapter 3 is presented. This new simulation has broad-band noise exterior to the narrow band-pass filters in addition to the broadband signal. The noises at each of the sensors in uncorrelated. The net effect of adding this noise is apparent in the discussion of the covariance. The autocorrelation of the noise sequence is the same in shape as the autocorrelation of the signal, but its magnitude is scaled by the signal-to-noise ratio. The effect this has on the covariance is that block diagonal components are added to the covariance which are scaled versions of the blocks given by the covariance of the signal alone. Only the diagonal blocks exist since the noises are uncorrelated between sensors.

It is found that the covariance becomes almost singular for certain bearings. This occurs for bearing angles for which the signal propagation delay between sensors is equal to or an integer multiple of the sampling interval.

Chapter 4 moves on into the area of bearing estimation using various estimation techniques. The two estimates that are discussed are the minimum mean square error method (MMSE) and the maximum a posteriori estimation (MAP) method. These estimates are made for an array of two sensors with quarter wavelength spacing between sensors for various sampling schemes. It is found that for a large number of data sets (400) the MAP and MMSE estimates are close to one another and that as the number of samples increases, or as the frequency of samples increases, the estimates become more reflective of the actual direction of arrival. It is also seen that the curves for the MAP and MMSE estimates intersect at a point around $\pm 60°$. This indicates that the density functions become skewed and are no longer close to Gaussian.

In order to better understand the trends seen in the estimate curves, other statistics such as the variances on the estimates are investigated. These variances are shown to have various trends according to the sampling scheme used to calculate the density functions. The sampling scheme referred to Nyquist sampling has differing trends for various estimates. The trend for MAP estimation is that the variance curve as a function of bearing increases up until about 60°. The variances then get smaller until

$\pm 90°$. This occurs since the densities are limited by a uniform distribution multiplier which effectively limits the densities between the ranges of $\pm \pi/2$. The MMSE curves have a peak in their variance curve at approximately $\pm 30°$. The variances then drop off as the bearing approaches $\pm 90°$. As the number of samples is increased and the sampling interval is decreased, low points or 'dips' occur in the variance curves for both the MMSE and MAP estimate variance curves. These 'dips' occur at exactly the points mentioned above as the points where the covariance matrices become singular.

The next measure of the accuracy of the estimates is the Cramer-Rao lower bound on the variance of estimates. The Cramer-Rao bound (C-R) is introduces as the variance of an estimator which is optimum and unbiased. The C-R bound is used to compare the estimates made using the density functions calculated in the thesis to estimates which would be made by an optimum estimator using the same covariance of the data. The trends which appear in the plots of the C-R bound vs. bearing angle are similar to those which appear in the MMSE and MAP estimate variances which appear above. In the case of Nyquist sampling, the trend is that the C-R bound as a function of bearing steadily increases until approximately $\pm 65°$. The curve then drops off until $90°$. As the number of samples or frequency of sampling is increased, again, 'dips' occur in the C-R lower bound curves. These 'dips' occur precisely those points mentioned above, where the covariance of the data becomes almost singular.

5.3 Recommendations for Further Research

In this section a few ideas for further research are presented. The problem of direction of arrival of a signal relative to an array of sensors has had many proposed solutions. Many algorithms have been presents for the solution of the problem. The object of this section is not to suggest new algorithms, but how to use the results of the thesis in order to test the performance of algorithms which already exist. The C-R bound is often used as a performance test by comparing the estimate variance to the C-R lower bound. The estimates on the bearing angle made in this thesis are done using a different density function from that used in the C-R bound tests. The density functions calculated in this work are conditioned on the actual data received at by the array. The C-R densities used in calculating the bound are conditioned on an assumed value of bearing angle. The difference is subtle, but the result is that the estimate variances presented is Chapter 4 are an alternative test of performance.

The first recommendation is that a code be written which is efficient. The code presented in this thesis which computes the conditional probability density function has a very long run time. For each point in the curves which are presented in Chapter 4, a large quantity of CPU time is required. An efficient code in FORTRAN or ADA could significantly reduce the run time. If the run time were significantly reduced, runs could be done to calculate density functions conditioned on larger data

sets. In this thesis the largest data set consists of twenty points. It would by interesting to see what effect a large number of near-singularities occurring in the covariance matrix has on estimates of bearing and the corresponding variances on those estimates.

The next interesting area of research would be to use the algorithm developed to calculate the conditional density function of the bearing angle for real data rather than simulated data. Some modifications to the code may me necessary to include possible noise correlation effects between sensors. The algorithm should also include more than two sensors. The work done above used only two sensors due to limited computing resources. It would be interesting to compute the density functions for real data for numerous sensors and compare the estimates of bearing angle made using the calculated densities vs. the bearing estimated using spectral or beamforming techniques discussed in Chapter 1.

Another interesting area of research would be to see what effect random sampling intervals would have on the density functions and the estimate variances. The effects on the covariance singularities and the related effects on the estimates would be interesting to see.

References

Bendat, Julius S. and Piersol, Allan G., "Random Data, Analysis and Measurement Procedures, Second Edition." John Wiley and Sons, New York (1986).

Burdic, William S., "Underwater Acoustic System Analysis." Prentice Hall, Englewood Cliffs, New Jersey (1984).

Hildebrand, Francis b., "Advanced Calculus for Applications." Prentice Hall, Englewood Cliffs, New Jersey (1976).

Law, Averill M., and Kelton W. David, "Simulation, Modeling and Analysis." McGraw Hill Book Company, New York (1982).

Rainal, A.J. "Monopulse Radars Excited by Gaussian Signals." IEEE Trans. on Aerospace and Electronic Systems, Vol. AES-2, No. 3, pp. 337-345 (May 1966).

Van Trees, Harry L., "Detection, Estimation, and Modulation Theory, Part 1." John Wiley and Sons, New York (1968).

Appendix A

The following is a listing of the code which generates the subblocks of the covariance matrix discussed in Chapter 2.

**The subroutine 'User' decides which subblock is to be filled then calles the necessary subroutines which fill the appropriate subblock.

```
      subroutine user(a,ma,g,s,t)
    real*8 a(1025,100),dpn,tau0,s,t,rs0(1025,1),tau(1025,1)
      integer n,pn,sens,sens1,l2,l3,ma,g
          n=a(1,3)
          pn=a(2,3)
          dpn=a(3,3)
          tau0=a(4,3)
          n0=a(5,3)
          sens=a(6,3)
          sens1=a(7,3)
          do 2 dd=1,1025,1
          tau(dd,1)=a(dd,2)
          rs0(dd,1)=a(dd,1)
          a(1,1)=rs0(513,1)
          a(2,2)=rs0(513,1)
          a(3,3)=rs0(513,1)
2         continue
          if (sens.eq.sens1) then
          call diagonal(n,pn,dpn,d,a,rs0,tau,n0)
          end if
          if (sens.lt.sens1) then
            do 40 l2=1,pn,1
              do 50 l3=1,pn,1
                if (l2.eq.l3) then
      call wow1 (l2,l3,tau0,sens,sens1,a,dpn,rs0,tau,n0)
                end if
               if (l2.lt.l3) then
      call wow2 (l2,l3,tau0,sens,sens1,a,dpn,rs0,tau,n0)
                end if
                if (l2.gt.l3) then
      call wow3 (l2,l3,tau0,sens,sens1,a,dpn,rs0,tau,n0)
```

```
                end if
50              continue
40              continue
            end if

            if (sens.gt.sens1) then
              do 60 l2=1,pn,1
                do 70 l3=1,pn,1
                  if (l2.eq.l3) then
      call wow4 (l2,l3,tau0,sens,sens1,a,dpn,rs0,tau,n0)
                  end if
                  if (l2.lt.l3) then
      call wow5 (l2,l3,tau0,sens,sens1,a,dpn,rs0,tau,n0)
                  end if
                  if (l2.gt.l3) then
      call wow6 (l2,l3,tau0,sens,sens1,a,dpn,rs0,tau,n0)
                  end if
70              continue
60              continue
            end if
           return
          end
```

** The subroutine 'Wow1' fills the main diagonals of the subblocks which lie below the main diagonal subblocks.

```
      subroutine wow1(l2,l3,tau0,sens,sens1,a,dpn,rs0,tau,n0)
      real*8 block(200,200),tau0,a(1025,100),dpn,rs0(1025,1),
     #tau(1025,1)
       integer n0,sens,sens1,jl,jh,jm,j,l2,l3
       block(l3,l2)=(sens1-sens)*tau0
       jh=n0
       jl=1
       jm=int((jh-jl)/2)
        do While ((jh-jl) .gt. 1)
           if (block(l3,l2).gt.tau(jm,1)) then
              jl=jm
              jm=int(jm+((jh-jl)/2))
             else
              jh=jm
              jm=int(jm-((jh-jl)/2))
           end if
         end do
```

```
      j=jl
      a(l3,l2)=((Rs0(j+1,1)-rs0(j,1))/(tau(j+1,1)-tau(j,1)))*
#(block(l3,l2)-tau(j,1))+rs0(j,1)
    return
    end
```

** The subroutine 'Wow2' fills the area below the main diagonal of the subblocks which lie below the main diagonal subblocks.

```
  subroutine wow2(l2,l3,tau0,sens,sens1,a,dpn,rs0,tau,n0)
  real*8 a(1025,100),block(200,200),tau0,dpn,rs0(1025,1),
#tau(1025,1)
    integer sens,sens1,l2,l3,n0,jh,jl,jm,j
   block(l3,l2)=((sens1-sens)*tau0)+((l3-l2)*dpn)
   jh=n0
   jl=1
   jm=int((jh-jl)/2)
    do While ((jh-jl) .gt. 1)
       if (block(l3,l2) .gt. tau(jm,1)) then
          jl=jm
          jm=int(jm+((jh-jl)/2))
         else
          jh=jm
          jm=int(jm-((jh-jl)/2))
       end if
     end do
      j=jl
      a(l3,l2)=((Rs0(j+1,1)-rs0(j,1))/(tau(j+1,1)-tau(j,1)))*
#(block(l3,l2)-tau(j,1))+rs0(j,1)
    return
    end
```

** The subroutine 'Wow3' fills the area above the main diagonal of the subblocks which lie below the main diagonal subblocks.

```
      subroutine wow3(l2,l3,tau0,sens,sens1,a,dpn,rs0,tau,n0)
        real*8 block(200,200),tau0,a(1025,100),dpn,rs0(1025,1),
     #tau(1025,1)
         integer sens,sens1,l2,l3,n0,jh,jm,j,jl
        block(l3,l2)=((sens1-sens)*tau0)-((l2-l3)*dpn)
        jh=n0
        jl=1
        jm=int((jh-jl)/2)
         do While ((jh-jl) .gt. 1)
            if (block(l3,l2) .gt. tau(jm,1)) then
               jl=jm
               jm=int(jm+((jh-jl)/2))
              else
               jh=jm
               jm=int(jm-((jh-jl)/2))
            end if
          end do
           j=jl
           a(l3,l2)=((Rs0(j+1,1)-rs0(j,1))/(tau(j+1,1)-tau(j,1)))*
     #(block(l3,l2)-tau(j,1))+rs0(j,1)
         return
         end
```

** The subroutine 'Wow4' fills the main diagonals of the subblocks which lie above the main diagonal subblocks.

```
      subroutine wow4(l2,l3,tau0,sens,sens1,a,dpn,rs0,tau,n0)
        real*8 block(200,200),tau0,a(1025,100),dpn,rs0(1025,1),
     #tau(1025,1)
        integer sens,sens1,l2,l3,n0,jh,jl,jm,j
        block(l3,l2)=((sens-sens1)*tau0)
        jh=n0
        jl=1
        jm=int((jh-jl)/2)
         do While ((jh-jl) .gt. 1)
            if (block(l3,l2) .gt. tau(jm,1)) then
               jl=jm
               jm=int(jm+((jh-jl)/2))
```

```
          else
           jh=jm
           jm=int(jm-((jh-jl)/2))
         end if
       end do
         j=jl
         a(l2,l3)=((Rs0(j+1,1)-rs0(j,1))/(tau(j+1,1)-tau(j,1)))*
#(block(l3,l2)-tau(j,1))+rs0(j,1)
      return
      end
```

** The subroutine 'Wow5' fills the area below the main diagonal of the subblocks which lie below the main diagonal subblocks.

```
      subroutine wow5(l2,l3,tau0,sens,sens1,a,dpn,rs0,tau,n0)
       real*8 block(200,200),tau0,a(1025,100),dpn,rs0(1025,1),
      #tau(1025,1)
        integer sens,sens1,l2,l3,n0,jh,jl,jm,j
        block(l3,l2)=((sens-sens1)*tau0)+((l3-l2)*dpn)
        jh=n0
        jl=1
        jm=int((jh-jl)/2)
         do While ((jh-jl) .gt. 1)
            if (block(l3,l2) .gt. tau(jm,1)) then
               jl=jm
               jm=int(jm+((jh-jl)/2))
              else
               jh=jm
               jm=int(jm-((jh-jl)/2))
           end if
         end do
           j=jl
           a(l2,l3)=((Rs0(j+1,1)-rs0(j,1))/(tau(j+1,1)-tau(j,1)))*
      #(block(l3,l2)-tau(j,1))+rs0(j,1)
         return
         end
```

** The subroutine 'Wow6' fills the area below the main diagonal of the subblocks which lie below the main diagonal subblocks.

```
      subroutine wow6(l2,l3,tau0,sens,sens1,a,dpn,rs0,tau,n0)
      real*8 block(200,200),tau0,a(1025,100),dpn,rs0(1025,1),
     #tau(1025,1)
      integer sens,sens1,l2,l3,n0,jh,jl,jm,j
      block(l3,l2)=((sens-sens1)*tau0)+((l3-l2)*dpn)
      jh=n0
      jl=1
      jm=int((jh-jl)/2)
       do While ((jh-jl) .gt. 1)
          if (block(l3,l2) .gt. tau(jm,1)) then
             jl=jm
             jm=int(jm+((jh-jl)/2))
            else
             jh=jm
             jm=int(jm-((jh-jl)/2))
          end if
        end do
          j=jl
     a(l2,l3)=((Rs0(j+1,1)-rs0(j,1))/(tau(j+1,1)-tau(j,1)))*
     #(block(l3,l2)-tau(j,1))+rs0(j,1)
       return
       end
```

** The subroutine 'Diagonal fills the main diagonal subblocks.

```
      subroutine  diagonal(n,pn,dpn,d,a,rs0,tau,n0)
       real*8 delay(2,1),d(200,200),dpn,a(1025,100),
      #rs0(1025,1),tau(1025,1)
       integer n,pn,sn,shift,n0,jh,jl,jm,j,czap,rzap
       do 10 b_column=1,n,1
        do 20 b_row=1,n,1
          sn=0
          if (b_row.eq.b_column) then
             do 25 11=1,pn,1
                Delay(11,1)=(11*dpn)-dpn
25           continue
       shift=b_column-1
              do 30 column=1,pn
```

```
            do 40 row=2,pn-sn
          czap=column+b_colum  !+shift
          rzap=b_row+row+sn+shift-1
          d(rzap,czap)=delay(row,1)
          d(czap,rzap)=delay(row,1)
        jl=1
        jh=n0
        jm=int((jh-jl)/2)
          do while ((jh-jl).gt.1)
            if (d(rzap,czap).gt.tau(jm,1)) then
              jl=jm
              jm=int(jm+((jh-jl)/2))
             else
              jh=jm
              jm=int(jm-((jh-jl)/2))
            end if
          end do
      a(rzap,czap)=((Rs0(jl+1,1)-rs0(jl,1))/(tau(jl+1,1)-
tau(jl,1)))*
     #(d(rzap,czap)-tau(jl,1))+rs0(jl,1)
      a(czap,rzap)=((Rs0(jl+1,1)-rs0(jl,1))/(tau(jl+1,1)-
tau(jl,1)))*
     #(d(rzap,czap)-tau(jl,1))+rs0(jl,1)
40          continue
           sn=sn+1
30          continue
           end if
20        continue
10        continue
        return
        end
```

Appendix B: Confidence Intervals

In this appendix, the method used to calculate the confidence intervals used in chapter 4 are discussed. The confidence intervals are used in Chapter 4 since the discussion covers calculations of statistics using large data sets. The discussion which follows gives a brief description of the method used to calculate confidence intervals which have 90% coverage on calculate parameters.

For a given set of data X_1, X_2, X_3, ..., X_n, with a finite mean μ and sample variance $s^2(n)$, the confidence interval based on the t distribution for large n is given by

$$CI = \bar{X} \pm z_{(1-\frac{\alpha}{2})} \sqrt{\frac{s^2(n)}{n}} \qquad (1)$$

The parameter α is determined by the percent confidence interval given by $100(1-\alpha)$. The parameter $z_{(1-\alpha/2)}$ is the upper $1-\alpha/2$ critical point for a standard normal distribution. See table T.1 of [1]. The interpretation of the confidence interval as given by (1) is as given by [1]

"If one constructs a very large number of $100(1-\alpha)$ percent confidence intervals each based on n observations, where n is sufficiently large, the proportion of these confidence intervals which contain (cover) μ should be $(1-\alpha)$. This proportion is called the coverage for the confidence interval."